Frechet derivatives of coupled seismograms with respect to an anelastic rotating earth

Eric Clévédé, Philippe Lognonné

Geophys. J. Int. (1996) **124**, 456–482

Fréchet derivatives of coupled seismograms with respect to an anelastic rotating earth

Eric Clévédé and Philippe Lognonné

Institut de Physique du Globe de Paris, Département de sismologie, URA CNRS 195, 4 *place Jussieu,* 75252 *Paris cedex* 05, *France*

Accepted 1995 August 23. Received 1995 August 18; in original form 1994 October 6

SUMMARY

A theory, based on higher-order perturbations, is given and used to express the partial derivatives of the seismic waveform with respect to perturbations of density, anelasticity and anisotropy. Fréchet derivatives are expressed with respect to a general aspherical model by using modulation functions, which are already used for the computation of aspherical seismograms. A direct solution method (DSM) that optimizes other previously proposed DSMs is proposed for the computation of the modulation functions.

Numerical tests point out significant differences between the general Fréchet derivatives and those used for more classical approaches (great-circle average or frozen-path approximation), as well as important focusing/defocusing effects. This theory will enable future imaging inversions of the small-scale heterogeneities of the Earth.

Key words: anelasticity, Fréchet derivatives, mode coupling, normal modes, perturbation methods, synthetic seismograms.

1 INTRODUCTION

The first large-scale inversions of seismic waveforms and the generation of 3-D tomographic models began in the 1980s: the Fréchet derivatives with respect to elastic lateral variations in a spherical earth model were derived by Woodhouse & Girnius (1982), and many inversions with respect to a spherical earth were subsequently performed. Most inversions were performed with simplifying assumptions in order to reduce the otherwise huge numerical task.

A first type of approximation is to invert seismic waveforms in a spherically symmetric earth model; structure below a great-circle path is inverted for each source–station path, in order to deduce *a posteriori* a 3-D model (e.g. Nolet, Van Trier & Huisman 1986; Nolet 1993; Stutzmann & Montagner 1993). If 3-D structure is taken into account *a priori* in the modelling, some simplifications are none the less necessary: Tanimoto (1984) only took into account self-coupling in a non-rotating elastic earth, and Woodhouse & Dziewonski (1984) performed waveform fitting by perturbing only the phase, in the context of an asymptotic theory. A further method investigated was the inversion of normal-mode spectra using isolated multiplets (Ritzwoller, Masters & Gilbert 1986, 1988; Giardini, Li & Woodhouse 1987, 1988). All of these inversions have been carried out in the context of a spherically homogeneous earth starting model.

Improvements in seismic data quality, as well as in our knowledge of lateral heterogeneity, warrant the use of new methods that can model lateral heterogeneities of different types: attenuation, anisotropy, and physical dispersion. Some improvements in the theory of global waveform modelling and inversion are described, in the framework of asymptotic theories, by Romanowicz (1987), Park (1987), Tromp & Dalhen (1922a, 1992b, 1993), Li & Romanowicz (1995). They allow the inversion of stronger smooth lateral variations of the Earth, of both elastic and anelastic structure. These methods, however, are not able to model the effect on the waveform of small-scale heterogeneities, which may be superimposed on the smooth structure already obtained by seismic inversions. Such small scales may have a significant effect on the amplitudes of normal modes (Park 1989; Lognonné & Romanowicz 1990a) and will provide new insights into Earth mantle dynamics. Fully coupled normal-mode methods are then necessary. For variational methods, Hara, Tsuboi & Geller (1991, 1993) and Geller & Hara (1993) proposed a direct solution method (DSM), where the seismograms and their Fréchet derivatives are computed directly, without computing the normal modes, and where the inversion is done with respect to a laterally heterogeneous earth. In order to reduce the computation time, however, the inversion is only done for a small number of modes around a frequency window centred on the inverted mode's frequency, and coupling between modes is modelled only between the modes contained in each of these windows. The computation time, together with the data distribution, is a main limitation of all waveform inversions, even on GigaFlop-class supercomputers.

To formulate a feasible approach for inversions able to retrieve the small-scale structure of the Earth, some important points must be appreciated. The first one is related to the fact that the Earth has only a small departure from spherical

symmetry, but that this departure is too great for linearized modelling techniques, such as the Born approximation or first-order perturbation theory. In practice, this means that most of the time properties of seismograms, such as traveltimes of body waves, dispersion curves of surface waves or resonant frequencies of normal modes, are dominated by the spherical structure. As a consequence, many 3-D waveform techniques such as ray tracing, finite differences, frequency-domain modal summations, or direct frequency methods such as the one used by Geller & Hara (1993), are, with the exception of symmetries, more constrained by the well-known spherical structure than by the aspherical structure of the Earth. This is not the case for methods where the departure of the observed seismic signal with respect to that of a spherical earth is modelled directly (e.g. differential traveltimes, splitting of normal modes, etc.). A good example may be found in the impact of lateral heterogeneities on normal modes, in the time domain rather than in the frquency domain. In that domain, the splitting produces a slow modulation, which has a characteristic time-scale that is typically 10 to 1000 times greater than the period of the mode. Direct-time finite-difference modelling of these slow modulations will thus require 10 to 1000 times smaller time steps than those which model the same effect, superimposed on the spherical structure. In the same way, a numerical error of the order of one per cent on the aspherical amplitude modulation is acceptable, when an error of one per cent on the spherical part of the signal, that is the fast-oscillating carrier, is not: such error has the same order of magnitude as the aspherical information.

A second point is that the number of major computations, particularly the computation of the partial derivatives must not grow as the product of the number of sources and stations. This was noted by Geller & Hara (1993), and for their direct frequency method the number of operations grows only as the number of earthquakes plus the number of stations; they have therefore partially solved the huge task of computing the perturbation of the seismograms.

These two points have also been recently addressed by Li & Romanowicz (1995). They separate the average frequency shift from higher perturbations, and reduce the number of computations by appropriately isolating the source and receiver functions.

The inversion theory we propose in this paper addresses these two constrains, and optimizes the inverse problem in the same way as the higher-order perturbation theory (Lognonné & Romanowicz 1990; Lognonné 1991) may optimize the forward variational problem. Moreover, as in Lognonné (1991), the formulation is, to third order, exact for lateral variations in anelasticity, anisotropy and physical dispersion of the Earth. In the first of a series of papers, we focus here on the Fréchet derivatives, that is the sensitivity of data with respect to 3-D lateral variations of elastic and anelastic parameters.

We first recall the solution in the aspherical case. Next we show how to compute seismograms with a direct solution method, and we express the formulation of the Fréchet derivatives of these seismograms for a general perturbation in elasticity, anelasticity and density. We will illustrate our results with some examples, showing the sensitivity of the amplitude and phase of the seismograms, as well as the trade-off between perturbations of the apparent attenuation of modes and focusing/defocusing effects.

2 THE SEISMIC EQUATION IN THE ROTATING ANELASTIC CASE

We first recall the theory of the forward problem, as described by Lognonné (1991). For that purpose, we start from the equation of motion of a rotating, elastic earth, obtained for example by Woodhouse & Dahlen (1978):

$$\partial_t^2|\mathbf{u}(t)\rangle - i\mathbf{B}\partial_t|\mathbf{u}(t)\rangle + \mathbf{A}|\mathbf{u}(t)\rangle = |\mathbf{f}(t)\rangle, \tag{1}$$

where $|\mathbf{u}(t)\rangle$ is the displacement field in braket notation, $|\mathbf{f}(t)\rangle$ is the equivalent body force for seismic sources and excitation terms, $\mathbf{A}$ is the elasto-dynamic operator and $\mathbf{B}$ the Coriolis operator, both defined in Woodhouse & Dahlen (1978) and Valette (1986). In all relations that follow, as in relation (1), all brakets and operators will implicitly depend on space. The generalization to the anelastic case is shown, for instance, by Liu, Anderson & Kanamori (1976), Dahlen (1981) or Tarantola (1988) and leads to a substitution of the relationship between the stress tensor τ_{ij} and strain ε^{kl} by a more general time convolution, which, in the case of local anelasticity, can be described using a generalized stiffness tensor C_{ijkl}. Taking the Fourier–Laplace transformation in braket notation, as

$$|\mathbf{u}(\sigma)\rangle = \int_0^{+\infty} \mathrm{e}^{i\sigma t}|\mathbf{u}(t)\rangle\, dt, \tag{2}$$

where $\sigma = \omega + i\alpha$ is the complex frequency in the upper part of the complex plane, we obtain an expression for the seismic equation (1) in the complex frequency domain:

$$-\sigma^2|\mathbf{u}(\sigma)\rangle + \sigma\mathbf{B}|\mathbf{u}(\sigma)\rangle + \mathbf{A}(\sigma)|\mathbf{u}(\sigma)\rangle = |\mathbf{f}(\sigma)\rangle = \mathscr{H}(\sigma)|\mathbf{u}(\sigma)\rangle, \tag{3}$$

where

$$\mathscr{H}(\sigma) = -\sigma^2 + \sigma\mathbf{B} + \mathbf{A}(\sigma)$$

is the elasto-dynamic operator in the frequency domain.

Lognonné (1991) has shown that this equation may be solved by using a normal-mode decomposition. However, it is not only necessary to use the normal modes of the primal equation, or right-normal modes, defined as

$$-\sigma_k^2|\mathbf{u}_k\rangle + \sigma_k\mathbf{B}|\mathbf{u}_k\rangle + \mathbf{A}(\sigma_k)|\mathbf{u}_k\rangle = 0, \tag{4}$$

but also the normal modes of the left-side problem, which, because the Coriolis and elasto-dynamic operators are anti-symmetric and symmetric respectively, are also the normal modes of the right-side problem with inverted rotation:

$$-\sigma_k^2|\mathbf{v}_k\rangle - \sigma_k\mathbf{B}|\mathbf{v}_k\rangle + \mathbf{A}(\sigma_k)|\mathbf{v}_k\rangle = 0. \tag{5}$$

The subscript k refers to the singlet eigenmode identified by the triplet (ℓ, n, m) where ℓ is the angular order of the mode, n its harmonic degree, and m its azimuthal order. The associated frequency is σ_k. In the following, K will denote the multiplet (ℓ, n) including the $2\ell+1$ singlets of same ℓ and n. σ_K will be the frequency of the spherical degenerate normal mode K.

Following Lognonné (1991), the response to a moment tensor source

$$|\mathbf{f}(t)\rangle = -H(t)\mathbf{M}\cdot\nabla\delta(\mathbf{r}-\mathbf{r}_s), \tag{6}$$

where $\mathbf{r}_s$ is the source location and $\mathbf{M}$ the moment tensor, is, for the displacement, given by

$$|\mathbf{u}(t)\rangle = H(t)\sum_{k>0}\mathscr{R}e\left\{\frac{1}{\sigma_k^2}\mathbf{M}:\nabla\mathbf{v}_k(\mathbf{r}_s)[1-\exp(i\sigma_k t)]|\mathbf{u}_k\rangle\right\}, \tag{7}$$

where $H(t)$ is the Heaviside distribution.

Let us now rewrite the latter expression by separating the spherical and aspherical parts of the signal. The modulation function of a multiplet K, defined as

$$|\mathbf{S}_K(t)\rangle = \sum_{k\in K} \mathbf{M}:\nabla\mathbf{v}_k(\mathbf{r}_s)\exp[i(\sigma_k-\sigma_K)t]|\mathbf{u}_k\rangle, \quad (8)$$

represents in space and time the acceleration of the ground produced by the mode K, demodulated from the spherical carrier frequency σ_K, and excited by the source. From eq. (7), it follows that the ground acceleration may be expressed as

$$|\ddot{\mathbf{u}}(t)\rangle = H(t)\sum_K \mathscr{R}e[\exp(i\sigma_K t)|\mathbf{S}_K(t)\rangle]. \quad (9)$$

Note that all seismograms excited by the same source can be expressed with the field described in relation (8). For example, the seismograms observed at a station with a receiver transfer function noted symbolically by $\langle\mathbf{R}|$ will simply be given by

$$s(t) = H(t)\sum_K \mathscr{R}e[\exp(i\sigma_K t)\langle\mathrm{R}|\mathbf{S}_K(t)\rangle]. \quad (10)$$

In the same way, it is possible to express all seismograms observed at a station, but produced by different earthquakes, with the same field: if we denote the source function by $|\mathbf{S}\rangle$, relation (8) can be rewritten as

$$|\mathbf{S}_K(t)\rangle = \sum_{k\in K}\exp[i(\sigma_k-\sigma_K)t]|\mathbf{u}_k\rangle\langle\mathbf{v}_k|\mathbf{S}\rangle, \quad (11)$$

where

$$|\mathbf{S}\rangle = -\mathbf{M}\cdot\nabla\delta(\mathbf{r}-\mathbf{r}_s).$$

Expression (10) then becomes

$$s(t) = H(t)\sum_K \mathscr{R}e[\exp(i\sigma_K t)\langle\mathbf{R}_K(t)|\mathbf{S}\rangle], \quad (12)$$

where

$$\langle\mathbf{R}_K(t)| = \sum_{k\in K}\exp[i(\sigma_k-\sigma_K)t]\langle\mathbf{R}|\mathbf{u}_k\rangle\langle\mathbf{v}_k|. \quad (13)$$

$\langle\mathbf{R}_K(t)|$ is equivalent to the acceleration of the ground produced by the mode K excited by a single Dirac force along the receiver axis and with a source time function given by the impulse response of the receiver instrument. We assume implicitly here that $\langle\mathbf{R}|$ has no pole at any eigenfrequency of the Earth when it is frequency-dependent, and that the operation $\langle\mathbf{R}|$ acting on the eigenmode $|\mathbf{u}_k\rangle$ is in fact given by

$$\langle\mathbf{R}|\mathbf{u}_k\rangle = \langle\mathbf{R}(\sigma_k)|\mathbf{u}_k\rangle.$$

The computation of $N\times M$ seismograms recorded on N stations and produced by M sources thus requires only the computation of N receiver modulation functions $\langle\mathbf{R}_K(t)|$ or M source modulation functions $|\mathbf{S}_K(t)\rangle$. In view, especially, of the limited number of stations used in global seismology, and their fixed character, this method provides a fast and optimal way to compute seismograms.

3 COMPUTING THE MODULATION FIELDS

The acceleration amplitude modulation field of the normal mode K can be computed by using the expression of normal modes given by Lognonné (1991). This, however, requires the computation of all singlets and, when coupling is taken into account, becomes a problem that is computationally demanding for angular orders higher than 100, especially if lateral variations of attenuation are introduced. We thus present here an alternative which does not involve the computation of normal modes. Let us recall the expression of a normal mode $|\mathbf{u}_k\rangle$, as given by Lognonné (1991), up to the second order of the perturbation theory for amplitudes, and third order for frequencies. Defining $\mathbf{K}_0$ as the identity operator in the eigenmode space, $\mathscr{S}_K$ as the subspace mapped by the $2\ell+1$ singlet k associated with the spherical multiplet K, and $\boldsymbol{\Delta}$ as the left inverse of the operator $[\mathscr{I}-\mathscr{P}][\mathbf{A}_0(\sigma_0)-\sigma_0^2\mathbf{K}_0][\mathscr{I}-\mathscr{P}]$, where $\mathscr{I}$ is the identity operator in $\mathscr{S}_K$ and $\mathscr{P}$ the projector on this subspace, we have

$$|\mathbf{u}_k\rangle = [1+\boldsymbol{\Delta}\boldsymbol{\delta}\mathbf{H}'+\boldsymbol{\Delta}\boldsymbol{\delta}\mathbf{H}'\boldsymbol{\Delta}\boldsymbol{\delta}\mathbf{H}']|\mathbf{u}_k^{(0)}\rangle + \delta_1\sigma_k\boldsymbol{\Delta}[\mathbf{B}'-2\sigma_0\boldsymbol{\delta}\mathbf{K}'-2\sigma_0\mathbf{K}_0\boldsymbol{\Delta}\boldsymbol{\delta}\mathbf{H}']|\mathbf{u}_k^{(0)}\rangle,$$

where

$$\boldsymbol{\delta}\mathbf{H}' = [\boldsymbol{\delta}\mathbf{A}(\sigma_0)+\sigma_0\mathbf{B}-\sigma_0^2\boldsymbol{\delta}\mathbf{K}],$$

$$\mathbf{B}' = \mathbf{B}+\partial_\sigma\mathbf{A}(\sigma_0)-\sigma_0\partial_\sigma^2\mathbf{A}(\sigma_0),$$

$$\mathbf{K}' = \mathbf{K}_0+\boldsymbol{\delta}\mathbf{K}-\frac{1}{2}\partial_\sigma^2\mathbf{A}(\sigma_0), \quad (14)$$

and where $|\mathbf{u}_k^{(0)}\rangle$ and $\delta_1\sigma_k$ are solutions of a $(2\ell+1)$-dimensional eigenproblem

$$\delta_1\sigma_k\mathbf{N}_0|\mathbf{u}_k^{(0)}\rangle = \boldsymbol{\delta}_1\mathbf{H}|\mathbf{u}_k^{(0)}\rangle, \quad (15)$$

in which $\mathbf{N}_0 = 2\sigma_0\mathbf{K}_0-\mathbf{B}_0$ and $\boldsymbol{\delta}_1\mathbf{H}$ is the first term of the power-series expansion of $\boldsymbol{\delta}\mathbf{H}'$ following the perturbation theory.

Let us now consider the field $|\mathbf{S}_K(t)\rangle$. This field can be rewritten as

$$|\mathbf{S}_K(t)\rangle = \mathscr{C}_K|\mathbf{S}_K^{(0)}(t)\rangle, \quad (16)$$

where the operator $\mathscr{C}_K$ is given by

$$\mathscr{C}_K = \mathbf{I}+\boldsymbol{\Delta}\boldsymbol{\delta}\mathbf{H}'+\boldsymbol{\Delta}\boldsymbol{\delta}\mathbf{H}'\boldsymbol{\Delta}\boldsymbol{\delta}\mathbf{H}' + [\mathbf{B}'-2\sigma_0\boldsymbol{\delta}\mathbf{K}'-2\sigma_0\mathbf{K}_0\boldsymbol{\Delta}\boldsymbol{\delta}\mathbf{H}']\mathbf{N}_0^{-1}\boldsymbol{\delta}_1\mathbf{H},$$

and where the field $|\mathbf{S}_K^{(0)}(t)\rangle$ is given by

$$|\mathbf{S}_K^{(0)}(t)\rangle = \sum_{k\in K}\exp[i(\sigma_k-\sigma_K)t]|\mathbf{u}_k^{(0)}\rangle\langle\mathbf{v}_k|\mathbf{S}\rangle, \quad (17)$$

with the initial value

$$|\mathbf{S}_K^{(0)}(0)\rangle = \left(\sum_{k\in K}|\mathbf{u}_k^{(0)}\rangle\langle\mathbf{v}_k\right)|\mathbf{S}\rangle. \quad (18)$$

As the eigenfunctions verify the orthogonality relation

$$\langle\mathbf{v}_k|\mathbf{N}_0\mathbf{u}_{k'}\rangle = \delta_{kk'}, \quad (19)$$

the initial value is simply

$$|\mathbf{S}_K^{(0)}(0)\rangle = \mathbf{N}_0^{-1}|\mathbf{S}\rangle. \quad (20)$$

We now apply the operator $\mathbf{N}_0$ to $|\mathbf{S}_K^{(0)}(t)\rangle$ and take a time derivative, thereby obtaining

$$\mathbf{N}_0\frac{\partial}{\partial t}|\mathbf{S}_K^{(0)}(t)\rangle = i\left(\boldsymbol{\delta}_1\mathbf{H}-\frac{\boldsymbol{\delta}_1\mathbf{H}\,\mathbf{N}_0^{-1}\boldsymbol{\delta}_1\mathbf{H}}{\sigma_K}\right)|\mathbf{S}_K^{(0)}(t)\rangle. \quad (21)$$

The source modulation field satisfies a differential equation of degree $2\ell+1$, which depends only on the aspherical structure. This equation (or its equivalent for the receiver) can be solved either in the time domain or in the frequency domain. Higher-

order finite differences can be used in the time domain, or an exact numerical method can be used in the frequency domain.

Eq. (21) can then be expressed with any basis of functions of $\mathcal{S}_K$, for example the $2\ell+1$ spherical singlets. In the same way, we can express the evolution of the receiver modulation function with the dual differential equation of (21). Note that for high values of ℓ, such as $2\ell+1$ is greater than the number of receivers used, this method is faster in terms of algorithm and operations than the method using the computation of the aspherical modes.

Eq. (21) and its dual equivalent are the basis of a direct solution method (DSM) for the modulation function. In contrast to the DSM proposed by Geller & Hara (1993), it is not based on the variational method but rather on the higher-order perturbation theory in the time domain. Both the size of the matrices involved and the number of time steps needed are reduced. This method then allows a very fast and yet accurate computation of all source and receiver modulation fields.

4 SEISMOGRAM PARTIAL DERIVATIVES

Let us now formulate the partial derivative of the seismograms with respect to a perturbation of the aspherical structure. In what follows, we will consider perturbations of the operator $\mathbf{A}(\sigma)$ only. Indeed, as shown by Lognonné & Romanowicz (1990b), the density perturbations can be renormalized to yield a renormalized operator $\mathbf{A}_r(\sigma)$. Perturbing the density with respect to the spherical density model then produces a perturbation of the operator $\mathbf{A}_r(\sigma)$ alone. We will also assume that the source is not perturbed. Starting from the elastodynamic equation (1), we easily obtain, after differentiation,

$$\mathscr{H}(\sigma)|\delta\mathbf{u}(\sigma)\rangle = -\delta\mathbf{A}(\sigma)|\mathbf{u}(\sigma)\rangle. \tag{22}$$

Substituting $|\mathbf{u}(\sigma)\rangle$ by its expression, we obtain

$$|\delta\mathbf{u}(\sigma)\rangle = -\mathscr{H}^{-1}(\sigma)\delta\mathbf{A}(\sigma)\mathscr{H}^{-1}(\sigma)|\mathbf{f}\rangle. \tag{23}$$

As for the seismograms, we want to express the Fréchet derivative wavefield by a superposition of normal modes of the current aspherical model. Note that these normal modes are not the spherical harmonic SNRAI (Spherical Non-Rotating Anelastic Isotropic) modes and will be updated after each iteration.

We then express $|\delta\mathbf{u}(\sigma)\rangle$ as

$$|\delta\mathbf{u}(\sigma)\rangle = \sum_k \delta c_k(\sigma)|\mathbf{u}_k\rangle. \tag{24}$$

Due to the dispersion (that is, the frequency dependence of the elasto-dynamic operator), the inverse of $\mathscr{H}(\sigma)$ is non-trivial. In the Fréchet derivatives we will, then, neglect the second-order terms with respect to the dispersion, so that $\mathscr{H}^{-1}(\sigma)$ may be approximated by

$$\mathscr{H}^{-1}(\sigma) = -\boldsymbol{\Upsilon}^{-1}(\sigma)\boldsymbol{\Lambda}^{-1}(\sigma)\{\mathbf{I}-[\mathbf{N}(\sigma)-\mathbf{I}]\}. \tag{25}$$

The corresponding matrix elements for $\mathbf{N}(\sigma)$ are

$$[\mathbf{N}(\sigma)]_{kk'} = \left\langle \mathbf{v}_{k'}\left|\mathbf{I}-\frac{1}{\sigma+\sigma_k}\left[\mathbf{B}+\frac{\mathbf{A}(\sigma)-\mathbf{A}(\sigma_k)}{\sigma-\sigma_k}\right]\right|\mathbf{u}_k\right\rangle, \tag{26}$$

and for $\boldsymbol{\Upsilon}(\sigma)$, $\boldsymbol{\Lambda}(\sigma)$ they are

$$[\boldsymbol{\Lambda}(\sigma)]_{kk'} = (\sigma-\sigma_k)\delta_{kk'}, \tag{27}$$

$$[\boldsymbol{\Upsilon}(\sigma)]_{kk'} = (\sigma+\sigma_k)\delta_{kk'}, \tag{28}$$

where $\delta_{kk'}$ is the Kronecker symbol.

From eqs (23) and (24), we finally obtain

$$\delta\bar{\mathbf{c}}(\sigma) = \delta\bar{\mathbf{c}}^{(1)}(\sigma) + \delta\bar{\mathbf{c}}^{(2)}(\sigma) + \delta\bar{\mathbf{c}}^{(3)}(\sigma), \tag{29}$$

with

$$\delta\bar{\mathbf{c}}^{(1)}(\sigma) = -\boldsymbol{\Upsilon}^{-1}(\sigma)\boldsymbol{\Lambda}^{-1}(\sigma)\delta\mathbf{A}(\sigma)\boldsymbol{\Upsilon}^{-1}(\sigma)\boldsymbol{\Lambda}^{-1}(\sigma)\bar{\mathbf{f}}, \tag{30}$$

$$\delta\bar{\mathbf{c}}^{(2)}(\sigma) = \boldsymbol{\Upsilon}^{-1}(\sigma)\boldsymbol{\Lambda}^{-1}(\sigma)[\mathbf{N}(\sigma)-\mathbf{I}]\delta\mathbf{A}(\sigma)\boldsymbol{\Upsilon}^{-1}(\sigma)\boldsymbol{\Lambda}^{-1}(\sigma)\bar{\mathbf{f}}, \tag{31}$$

$$\delta\bar{\mathbf{c}}^{(3)}(\sigma) = \boldsymbol{\Upsilon}^{-1}(\sigma)\boldsymbol{\Lambda}^{-1}(\sigma)\delta\mathbf{A}(\sigma)\boldsymbol{\Upsilon}^{-1}(\sigma)\boldsymbol{\Lambda}^{-1}(\sigma)[\mathbf{N}(\sigma)-\mathbf{I}]\bar{\mathbf{f}}. \tag{32}$$

$\delta\bar{\mathbf{c}}^{(1)}(\sigma)$ represents the main contribution of the Fréchet derivative, and $\delta\bar{\mathbf{c}}^{(2)}(\sigma)$ and $\delta\bar{\mathbf{c}}^{(3)}(\sigma)$ are significantly smaller: their ratio with respect to $\delta\bar{\mathbf{c}}^{(1)}(\sigma)$ is typically given by $1/Q$, where Q is the intrinsic quality factor. Their contribution to the overall Fréchet derivative is less than 1 per cent for typical Q of 100 or more.

Let us consider the term $\delta\bar{\mathbf{c}}^{(1)}(\sigma)$ and express it in time. Details of this first term are given in Appendix A. The contribution to the acceleration field of this term can be obtained by summing all singlets k of all multiplets K, so that we have

$$|\delta\ddot{\mathbf{u}}(t)\rangle = \sum_k \delta c_k^{(1),\mathrm{acc}}(t)|\mathbf{u}_k\rangle, \tag{33}$$

and the contribution for a single seismogram is simply

$$\delta s(t) = \sum_k \delta c_k^{(1),\mathrm{acc}}(t)\langle\mathbf{R}|\mathbf{u}_k\rangle, \tag{34}$$

where $\langle\mathbf{R}|$ is the receiver transfer function. As shown in Appendix A, the Fréchet derivative then needs a double summation for all singlets k and k', the first summation being in expression (34), and the second in (A6). We can write this derivative formally in a first step as

$$\delta s(t) = \sum_{K,K'} s_{K,K'}(t). \tag{35}$$

We consider separately the contribution $s_{K,K}$ involving the singlets k and k' of the same multiplet K (developed in Appendix B), and the contribution $s_{K,K'}$ involving the singlets k and k' of the multiplets K and K' respectively (see Appendix C). We can then rewrite the perturbation of the seismogram as a summation on perturbed modulation function multiplied by the unperturbed spherical frequency carrier, so that $\delta s(t)$ is given by

$$\delta s(t) = \sum_K \delta A_K(t)\exp(i\sigma_K t), \tag{36}$$

where we can write $\delta A_K(t)$ as the contribution of two terms:

$$\delta A_K(t) = \delta A_K^{\mathrm{s}}(t) + \delta A_K^{\mathrm{c}}(t). \tag{37}$$

The first term $\delta A_K^{\mathrm{s}}(t)$ is the perturbation of the modulation function due to self-coupling, and is deduced from relation (B4):

$$\begin{aligned}\delta A_K^{\mathrm{s}}(t) = \frac{-i}{4\sigma_K}\int_0^t &\langle\mathbf{R}_K(t-\tau)|\delta\mathbf{A}(\sigma_K)|\mathbf{S}_K(\tau)\rangle\,d\tau\\ &+\frac{1}{8\sigma_K^2}\int_0^t[\langle\dot{\mathbf{R}}_K(t-\tau)|\delta\mathbf{A}(\sigma_K)|\mathbf{S}_K(\tau)\rangle\\ &+\mathbf{R}_K(t-\tau)|\delta\mathbf{A}(\sigma_K)|\dot{\mathbf{S}}_K(\tau)\rangle]\,d\tau\\ &-\frac{1}{8\sigma_K}\int_0^t[\langle\dot{\mathbf{R}}_K(t-\tau)|\partial_\sigma\delta\mathbf{A}(\sigma_K)|\mathbf{S}_K(\tau)\rangle\\ &+\langle\mathbf{R}_K(t-\tau)|\partial_\sigma\delta\mathbf{A}(\sigma_K)|\dot{\mathbf{S}}_K(\tau)\rangle]\,d\tau\end{aligned}$$

$$
\begin{aligned}
&-\frac{1}{8\sigma_K}[\langle \mathbf{R}_K(t)|\partial_\sigma \boldsymbol{\delta}\mathbf{A}(\sigma_K)|\mathbf{S}_K(0)\rangle \\
&+\langle \mathbf{R}_K(0)|\partial_\sigma \boldsymbol{\delta}\mathbf{A}(\sigma_K)|\mathbf{S}_K(t)\rangle] \\
&-\frac{i}{16\sigma_K^2}[\langle \dot{\mathbf{R}}_K(t)|\partial_\sigma \boldsymbol{\delta}\mathbf{A}(\sigma_K)|\mathbf{S}_K(0)\rangle \\
&+\langle \dot{\mathbf{R}}_K(0)|\partial_\sigma \boldsymbol{\delta}\mathbf{A}(\sigma_K)|\mathbf{S}_K(t)\rangle] \\
&-\frac{i}{16\sigma_K^2}[\langle \mathbf{R}_K(t)|\partial_\sigma \boldsymbol{\delta}\mathbf{A}(\sigma_K)|\dot{\mathbf{S}}_K(0)\rangle \\
&+\langle \mathbf{R}_K(0)|\partial_\sigma \boldsymbol{\delta}\mathbf{A}(\sigma_K)|\dot{\mathbf{S}}_K(t)\rangle], \qquad (38)
\end{aligned}
$$

where $\langle \dot{\mathbf{R}}_K(t)|$ and $|\dot{\mathbf{S}}_K(t)\rangle$ are the time derivatives of $\langle \mathbf{R}_K(t)|$ and $|\mathbf{S}_K(t)\rangle$, respectively.

The second term is obtained from relation (C1) by summing all terms where the carrier $\exp(i\sigma_K t)$ appears. We then have

$$
\begin{aligned}
\delta A_K^c(t) = &\sum_{K' \neq K} \frac{1}{\sigma_{K'}^2 - \sigma_K^2}\{[\langle \mathbf{R}_K(t)|\boldsymbol{\delta}\mathbf{A}(\sigma_K)|\mathbf{S}_{K'}(0)\rangle \\
&+\langle \mathbf{R}_{K'}(0)|\boldsymbol{\delta}\mathbf{A}(\sigma_K)|\mathbf{S}_K(t)\rangle] \\
&+i[\langle \dot{\mathbf{R}}_K(t)|\partial_\sigma \boldsymbol{\delta}\mathbf{A}(\sigma_K)|\mathbf{S}_{K'}(0)\rangle \\
&+\langle \mathbf{R}_{K'}(0)|\partial_\sigma \boldsymbol{\delta}\mathbf{A}(\sigma_K)|\dot{\mathbf{S}}_K(t)\rangle]\} \\
&+\sum_{K' \neq K} \frac{1}{(\sigma_{K'}^2 - \sigma_K^2)^2}\{2i\sigma_{K'}[\langle \mathbf{R}_K(t)|\boldsymbol{\delta}\mathbf{A}(\sigma_K)|\dot{\mathbf{S}}_{K'}(0)\rangle \\
&+\langle \dot{\mathbf{R}}_{K'}(0)|\boldsymbol{\delta}\mathbf{A}(\sigma_K)|\mathbf{S}_K(t)\rangle] \\
&-2i\sigma_K[\langle \dot{\mathbf{R}}_K(t)|\boldsymbol{\delta}\mathbf{A}(\sigma_K)|\mathbf{S}_{K'}(0)\rangle \\
&+\langle \mathbf{R}_{K'}(0)|\boldsymbol{\delta}\mathbf{A}(\sigma_K)|\dot{\mathbf{S}}_K(t)\rangle]\}. \qquad (39)
\end{aligned}
$$

We now look at the two terms $\delta\bar{\mathbf{c}}^{(2)}(\sigma)$ and $\delta\bar{\mathbf{c}}^{(3)}(\sigma)$, due to the dispersive part. These terms, however, are quite similar to those described above, except that instead of $\boldsymbol{\delta}\mathbf{A}(\sigma_K)$ in relations (39) and (38), we have to substitute the term $\boldsymbol{\delta}\mathbf{A}(\sigma_K)[\mathbf{N}(\sigma)-\mathbf{I}]+[\mathbf{N}(\sigma)-\mathbf{I}]\boldsymbol{\delta}\mathbf{A}(\sigma_K)$, which includes the dispersive terms. Thus we need to express the space–time fields

$$
\langle \tilde{\mathbf{R}}_K(t)| = \sum_{k,k' \in K} \exp[i(\sigma_k - \sigma_K)t]\langle \mathbf{R}|\mathbf{u}_{k'}\rangle\langle \mathbf{v}_{k'}|\mathbf{N}(\sigma_K)|\mathbf{u}_k\rangle\langle \mathbf{v}_k| \qquad (40)
$$

and

$$
|\tilde{\mathbf{S}}_K(t)\rangle = \sum_{k,k' \in K} \exp[i(\sigma_k - \sigma_K)t]|\mathbf{u}_k\rangle\langle \mathbf{v}_k|\mathbf{N}(\sigma_K)|\mathbf{u}_{k'}\rangle\langle \mathbf{v}_{k'}|\mathbf{S}\rangle \qquad (41)
$$

that appear, along with their corresponding time derivatives, in the expressions (38) and (39).

Relations (38) and (39) generalize the Woodhouse & Girnius (1982) formulation when the Fréchet derivative is done with respect to a 3-D aspherical earth instead of a SNRAI spherical earth. Note in particular that all secular terms involve a convolution between the receiver and source modulation fields. For a Fréchet derivative with respect to a spherical model (having its eigenfrequency equal to the eigenfrequency used for the carrier), these two functions are non time-dependent, and all three convolutions in (38) reduce to the single term

$$
-\frac{i}{4\sigma_K}\langle \mathbf{R}|\boldsymbol{\delta}\mathbf{A}|\mathbf{S}\rangle t,
$$

i.e. the short time approximation of Jordan (1978). Note that relations (38) and (39) are fully symmetric with respect to the receiver and source functions. We note also the relative importance of the different terms in eq. (38): the three first lines are related to perturbation of the stiffness tensor, the second one being of the order of $\delta\sigma/\sigma$ while the first one is of order 1. The eight last lines are related to a perturbation in the physical dispersion of the Earth and involve both secular and non-secular terms. The first and second square brackets in the third integral represent the major contribution and the ratio between these two terms is of the order of $\delta\omega t$: this implies a predominance of the second term at the beginning of the signal, and after a time equal to the inverse of the splitting width, a predominance of the first, secular, term.

5 NUMERICAL TESTS

We present here some examples of modulation fields, on both the source and receiver, and express the Fréchet derivative of the recorded amplitude modulation. These examples are for two fundamental modes, ${}_0S_{52}$ and ${}_0S_{17}$. We then compute the instantaneous perturbation of the local frequency of these modes and discuss the trade-off between the perturbation of the apparent attenuation and focusing/defocusing effects. The numerical tests have been performed using the aspherical model M84A (Woodhouse & Dziewonski 1984), superimposed on the spherical model PREM (Dziewonski & Anderson 1981). The aspherical modes were computed up to third order of perturbation theory, taking into account all the coupling effects related to this model with lateral variations up to degree 8, which means with the 16 nearest multiplets. Only coupling along the dispersion branch was considered.

5.1 Modulation fields

Figs 1–3 show modulation fields at the receiver and source for the multiplet ${}_0S_{52}$. These fields are computed by making the inverse Legendre transformation of the hybrid modulation functions at the source and receiver [see Lognonné & Romanowicz (1990) for details on the discrete Legendre transformations]. These fields correspond to the vertical displacement at a depth of 500 km. Due to the small coupling and the smooth dependence of the spherical eigenfunction on ℓ, changes in depth mainly affect the amplitude of the modulation function and not it shape. The source is a double couple located at a depth of 15 km, along the equator, at 195°E. The mechanism of the source is a vertical strike-slip with a 45° strike. Fig. 1 shows the modulation function of the source at all positions on a 500 km deep sphere. Similarly, Fig. 2 shows the modulation function associated with the receiver. This function shows the amplitude recovered along the vertical axis at all points of the 500 km deep sphere for an impulsive source. At $t = 0$, these modulation functions only differ slightly from the spherical earth amplitude response. Differences arise only from coupling effects. When time increases, however, and in contrast to the spherical earth case, the modulation function varies, mainly due to the self-coupling; these variations are shown in Figs 3(a)–(d). Figs 3(a) and (b) show the real and imaginary parts of the source modulation field after 6 hr, while Figs 3(c) and (d) show these fields after 12 hr. In an aspherical earth, as noted by Dahlen & Henson (1985) and Henson & Dalhen (1986), the $2\ell+1$ eigenmode singlets have a significant ampli-

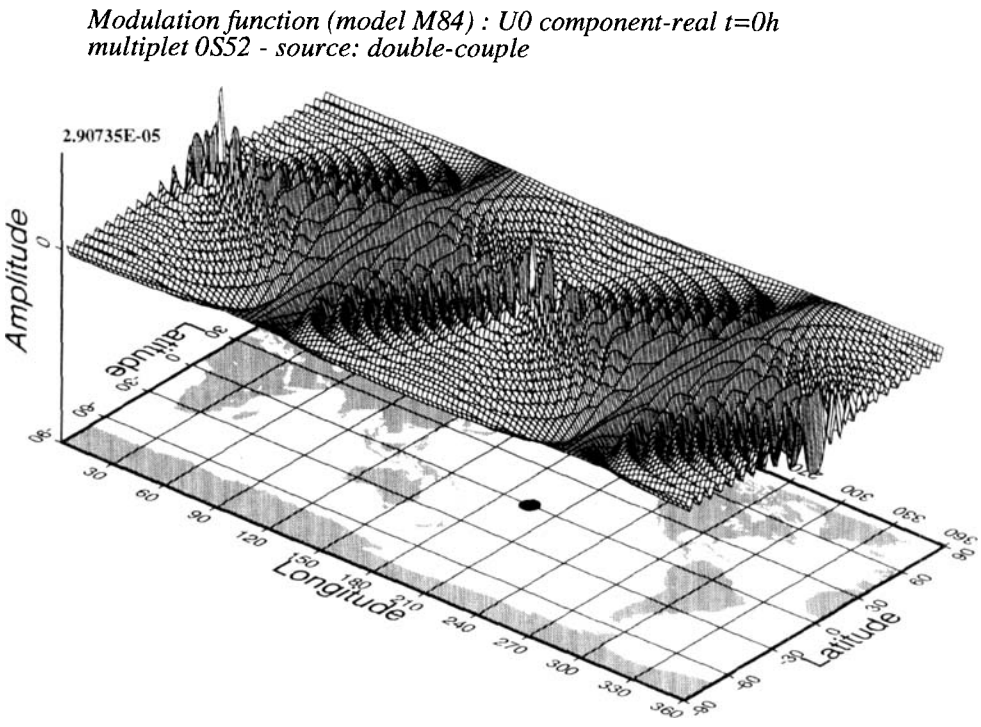

Figure 1. Modulation field at the source (double-couple) for the multiplet ${}_0S_{52}$, at time $t = 0$ hr. The vertical component U_0 is shown at a depth of 500 km. The source is a vertical strike slip with the fault plane oriented at 45° to the equator. Peaks are present at both the location of the source (0.10°N 195°E, 15 km depth, indicated by a black circle on the background map) and its antipode. At the initial time, the field is purely real and is close to the spherical case. This figure could be interpreted as the amplitude of vertical displacement associated with this source for all points on a 500 km depth sphere. For all figures the computation is done using the M84A model of Woodhouse & Dziewonski (1984).

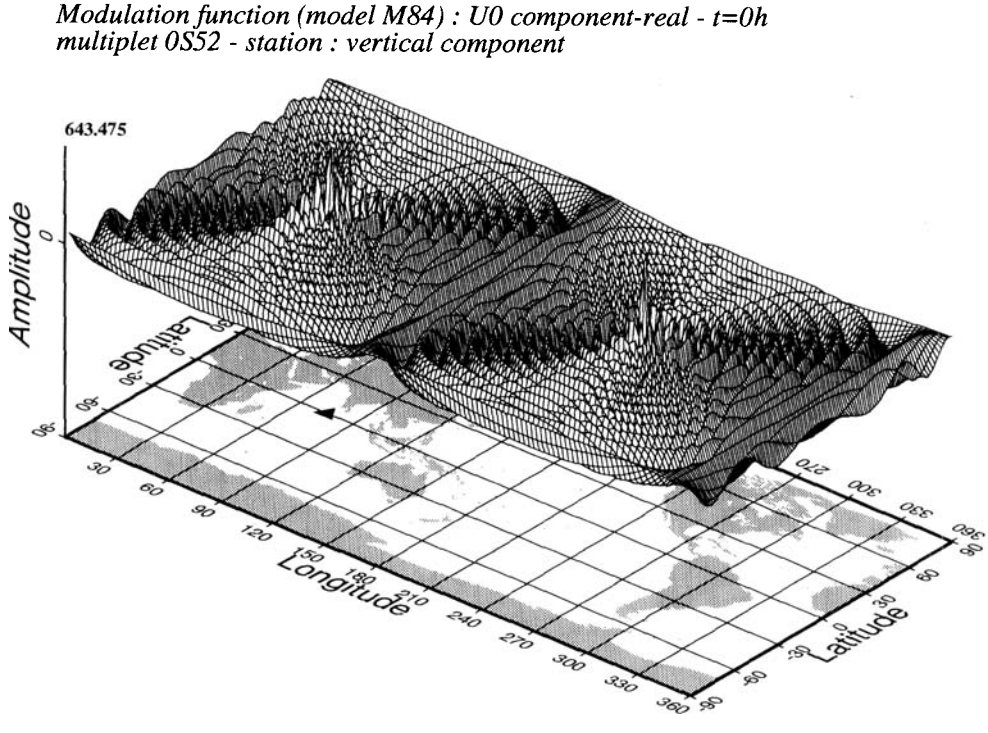

Figure 2. Modulation field at the station for the multiplet ${}_0S_{52}$, at time $t = 0$ hr. Depth is fixed at 500 km. As for Fig. 1, the U_0 component of the field is shown. Peaks are also present at both the receiver location (0.10°N 75°E, indicated by a black triangle on the background map) and its antipode. As in Fig. 1, the field is real and close to the spherical case. This figure gives the displacement recovered at the receiver for a vertical impulsive source for all points on a 500 km depth sphere. Note that the two peaks have the same sign, due to the even angular order of the mode (this is also true for Fig. 1).

(a) *Perturbation of the modulation function (model M84) : U0 component-real t=6h multiplet 0S52 - source: double-couple*

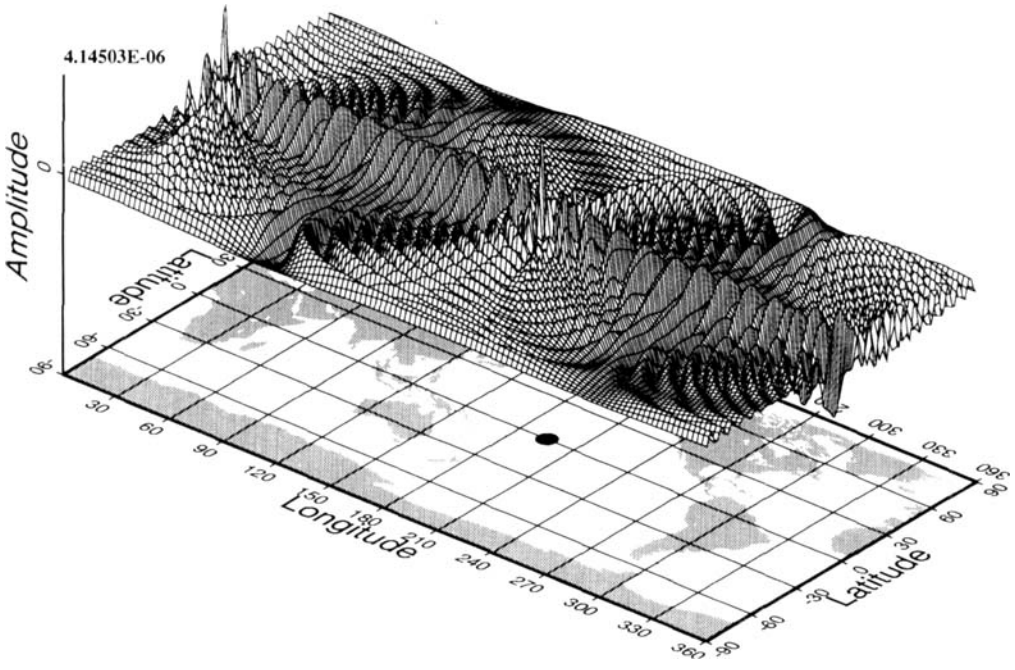

(b) *Perturbation of the modulation function (model M84) : U0 component-imaginary t=6h multiplet 0S52 - source: double-couple*

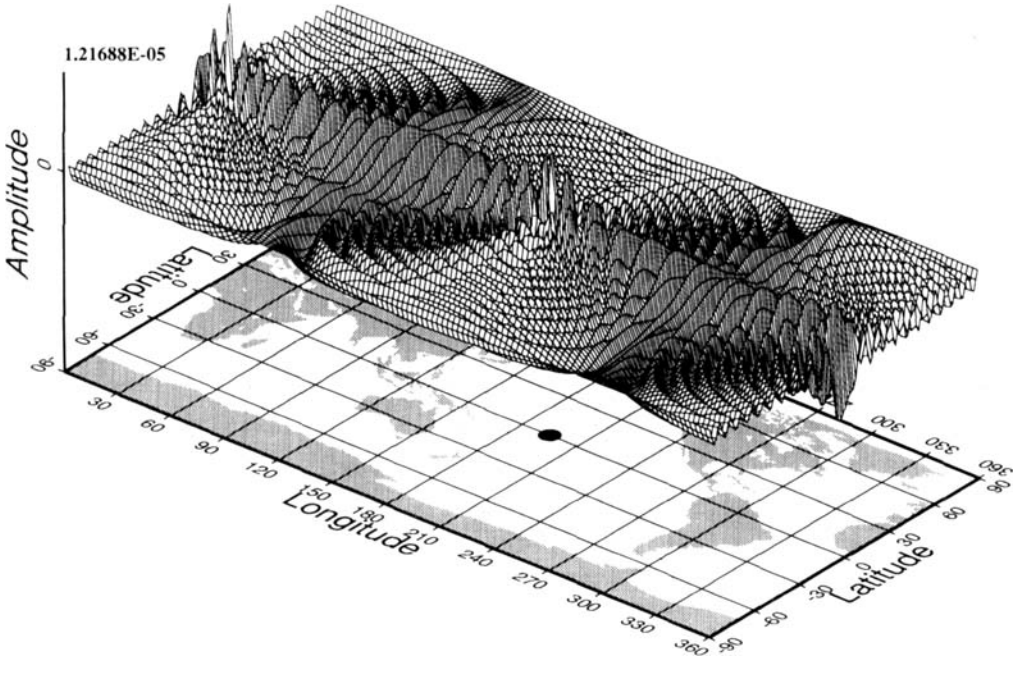

Figure 3. Perturbation of the modulation field at the source for the multiplet ${}_0S_{52}$, at times $t = 6$ hr and $t = 12$ hr. (a) ($t = 6$ hr) and (c) ($t = 12$ hr) show the real parts; the field of reference is the modulation at the initial instant (Fig. 1). In the spherical case, this difference is zero. (b) and (d) show the imaginary part of the modulation fields at times $t = 6$ hr and $t = 12$ hr respectively. These fields are equivalent to the absolute ones, since the imaginary part of the modulation field at the initial time is null.

(c) *Perturbation of the modulation function (model M84) : U0 component-real t=12h multiplet 0S52 - source: double-couple*

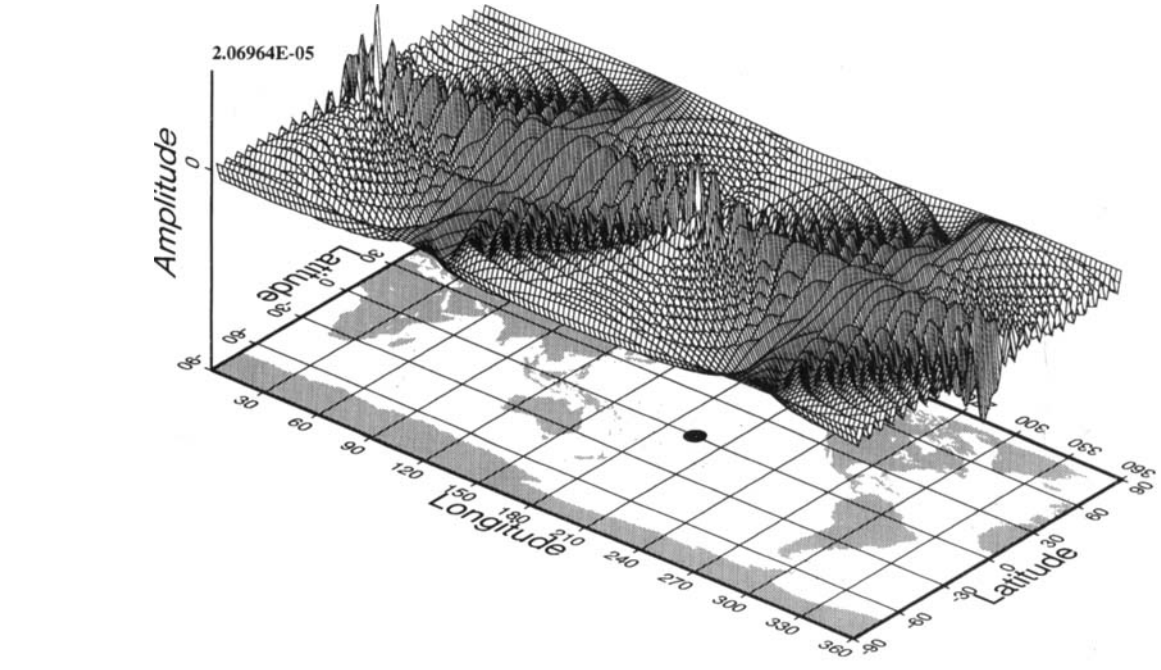

(d) *Perturbation of the modulation function (model M84) : U0 component-imaginary t=12h multiplet 0S52 - source: double-couple*

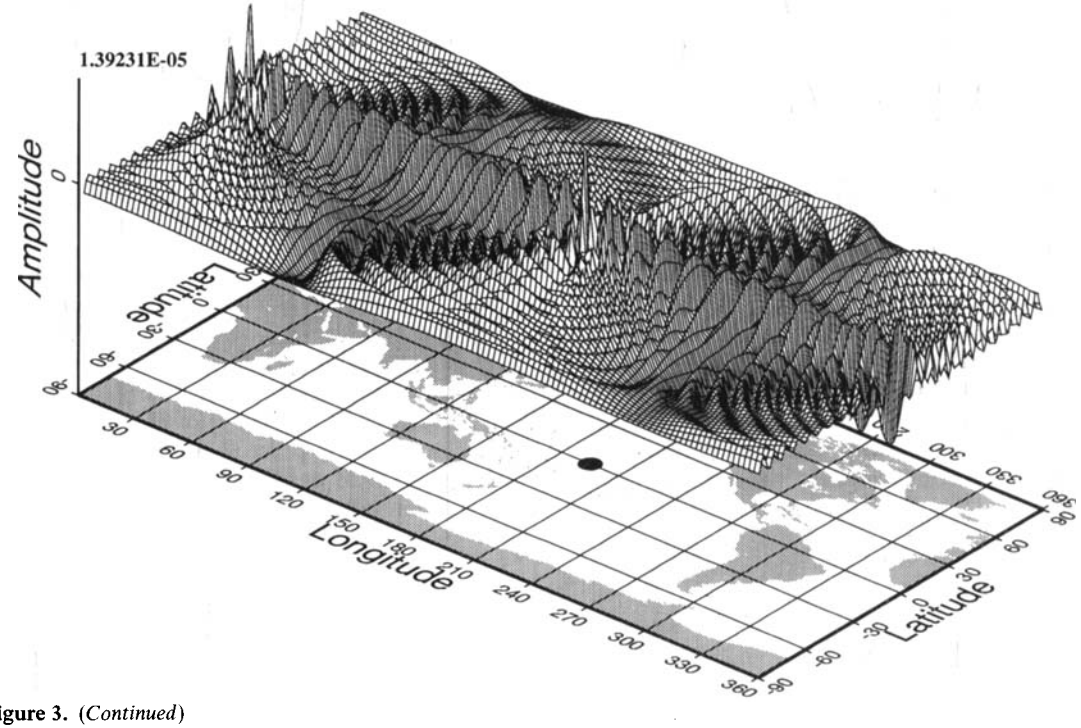

Figure 3. (*Continued*)

tude along $\ell+1$ great circles. Each great circle, except one, is associated with two modes with very close frequencies. Both modulation fields at the source and receiver then select the singlets that possess an antinode at the source or receiver location. As seen in Fig. 4, when the initial amplitudes of the singlets are plotted, only a few have a significant amplitude. As time increases, the departure from the sphericity of the earth induces slow variations of the initial amplitude. The perturbations with respect to the initial amplitude are concentrated along the singlet great circles with maximum amplitudes.

Note that the perturbation of the modulation function, i.e. its departure from a constant function, is quite significant. The perturbation represents 50 per cent of the initial value after 6 hr, and is equal to the initial field after 12 hr.

We have also computed the modulation field for an isotropic source. It looks, of course, like the modulation field at the receiver (which is also isotropic) when, as in the numerical example shown here, either no lateral variation in attenuation or no rotation is assumed, thus implying the same dual and primal eigenmodes.

5.2 Fréchet derivative kernel

The Fréchet derivatives involve modulation functions both at the source and receiver. These Fréchet derivative kernels are shown in Figs 5–6 for the mode ${}_0S_{52}$. In each of these figures, the amplitude at a given point with latitude θ and longitude ϕ is the perturbation in the recorded amplitude modulation function when a Dirac delta function perturbation is put in the model M84A at a depth of 500 km and at location θ, ϕ. Figs 5(a)–(f) and 6(a)–(f) are for perturbations in the shear modulus. In Figs 5(a)–(f), we show the Fréchet derivative obtained only by the self-coupling terms, which are given by relation (38). Note, however, that coupling is taken into account in the computation of normal modes, and in the computation of the modulation fields. At the initial time (Figs 5a and b), the kernel appears to have a maximum along the great circle (in our case the equator) connecting the source and the station. The phase plot shows that this 'equatorial peak' is a stationary phase point, giving rise to the asymptotic approximation of the great-circle path average. Our results diverge from the asymptotic approximation, however, by the

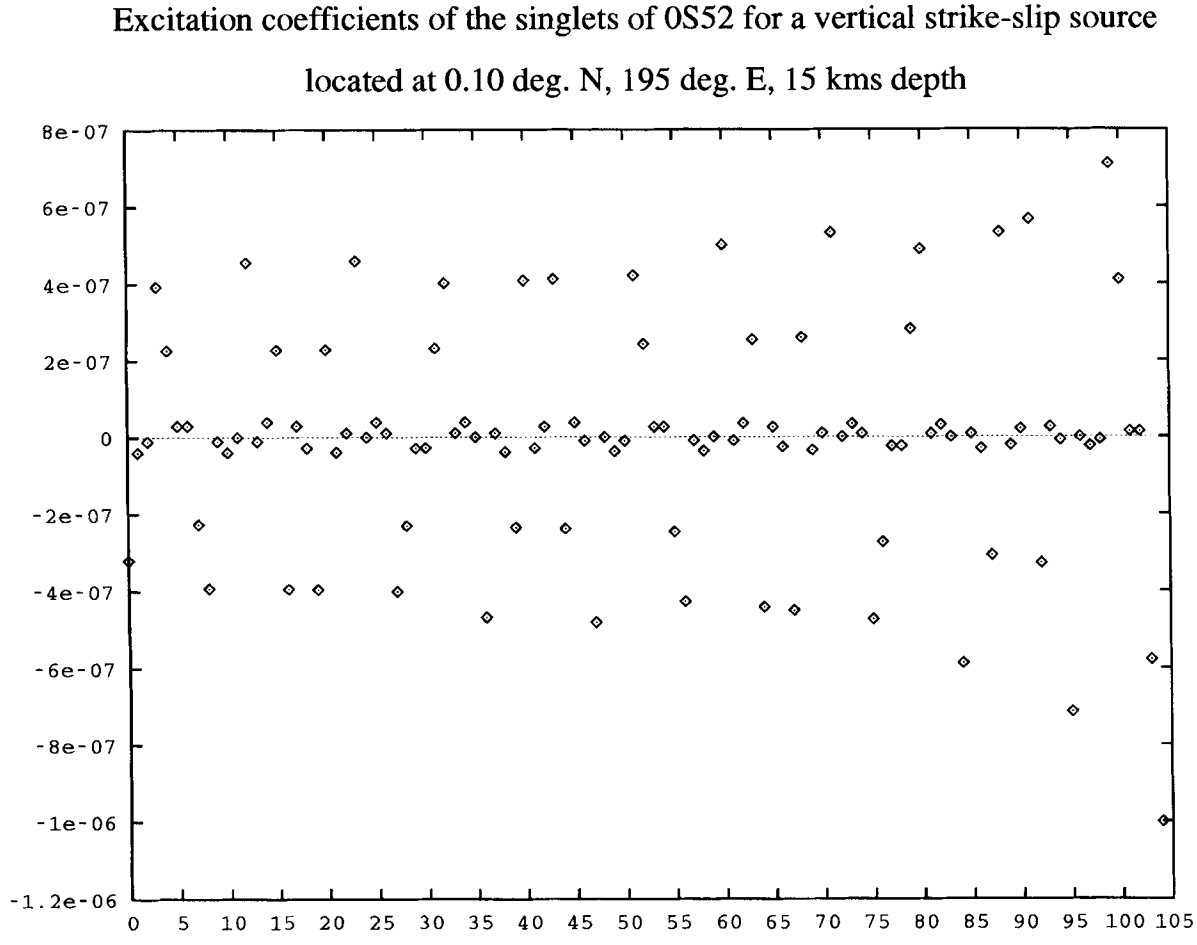

Figure 4. Excitation coefficients of the singlets of the multiplet ${}_0S_{52}$. The source is the vertical strike slip used for Figs 1, 2 and 3. The coefficients associated with the $2\ell+1$ singlets (e.g. 105 modes) are plotted in increasing frequency order. Only less than half of the singlets have a significant amplitude of excitation. The most excited singlets lead to the general pattern of the modulation field, as the great circles corresponding to these singlets are the locations of maximum amplitude.

(a) *Frechet derivative kernel (model M84) : amplitude - time=0h*
multiplet 0S52 : isolated
perturbation in μ (0.1%) - double-couple source / vertical instrument

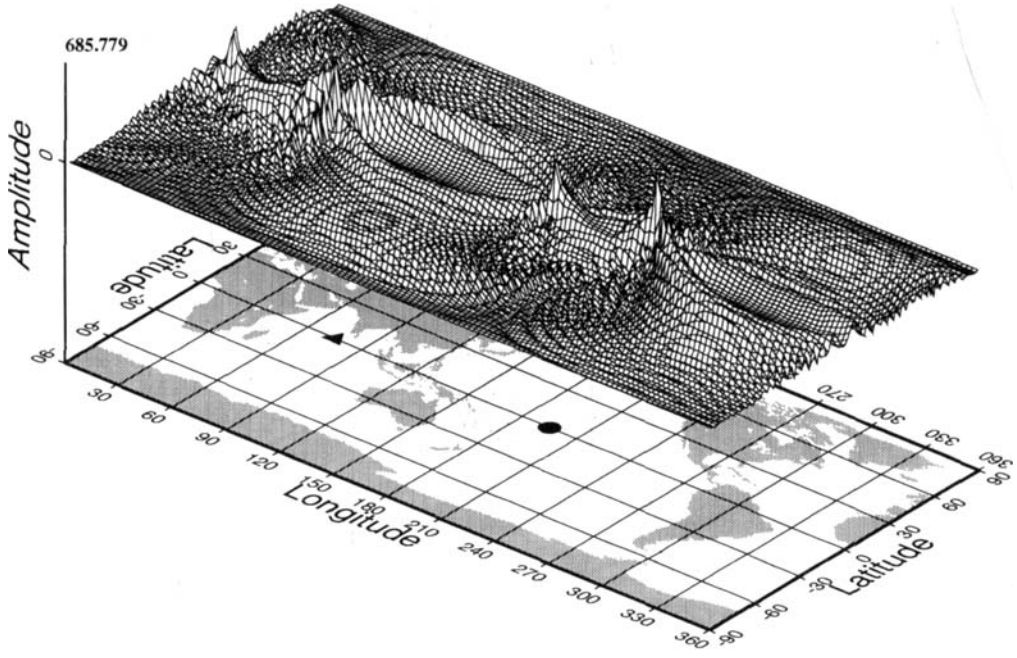

(b) *Frechet derivative kernel (model M84) : phase - time=0h*
multiplet 0S52 : isolated
perturbation in μ (0.1%) - double-couple source / vertical instrument

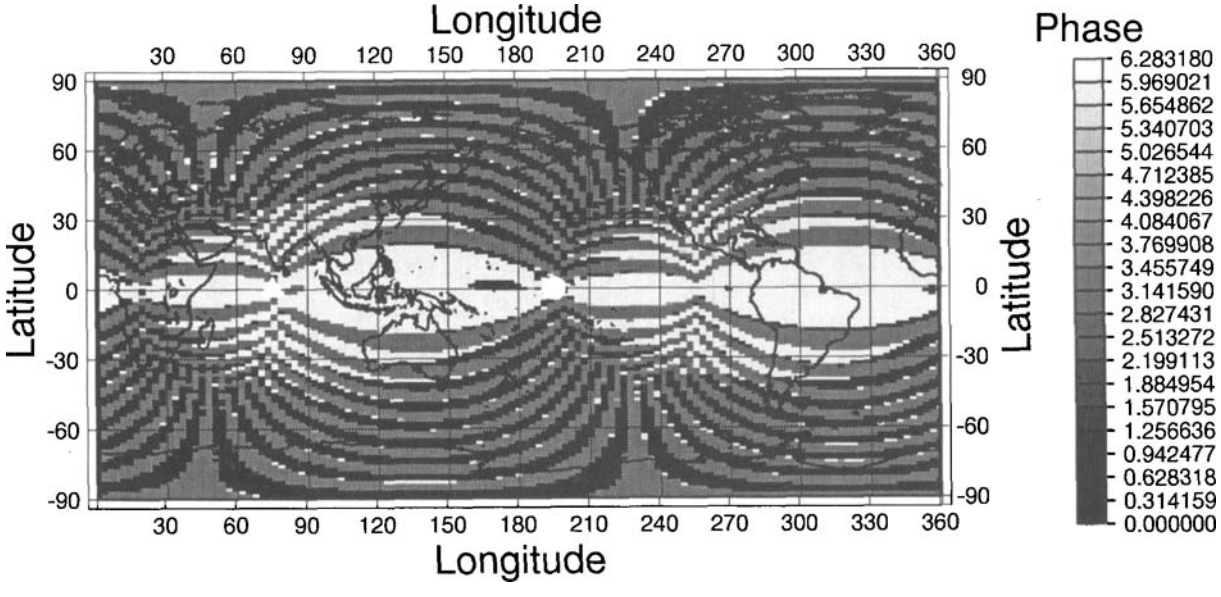

Figure 5. Isolated multiplet hypothesis: evolution of the Fréchet derivatives kernel (double-couple source) for ${}_0S_{52}$ for a perturbation in the shear modulus at several instants. The map shows, on all latitudes and longitudes, the perturbation of the recorded demodulated amplitude for the normal mode ${}_0S_{52}$, when a Dirac perturbation of 0.1 per cent of the spherical PREM value is put at the given latitude and longitude, and at a depth of 500 km. The source is the vertical strike slip used for Fig. 1. (a), (c) and (e) show the absolute amplitude of the kernel at times $t = 0$, 6 and 12 hr respectively. (b), (d) and (f) give the corresponding phase. On both the amplitude and phase representation, the source location (same as Fig. 1) is indicated by a circle on the background map, and the receiver location (same as Fig. 2) by a triangle. The phase representation is done so that white corresponds to zero, black to 2π, and median grey to π. Thus, whiter and darker zones correspond to close phases. Hence, (b) shows that, at the initial instant, the phase takes only values π and 0 (or 2π), so that the kernel is purely real. Moreover, we can see that the equatorial zone is a stationary phase point, as predicted by asymptotic results. In (d) and (f) the pattern changes as the kernels become fully complex.

(c) *Frechet derivative kernel (model M84) : amplitude - time=6h*
multiplet 0S52 : isolated
perturbation in μ (0.1%) - double-couple source / vertical instrument

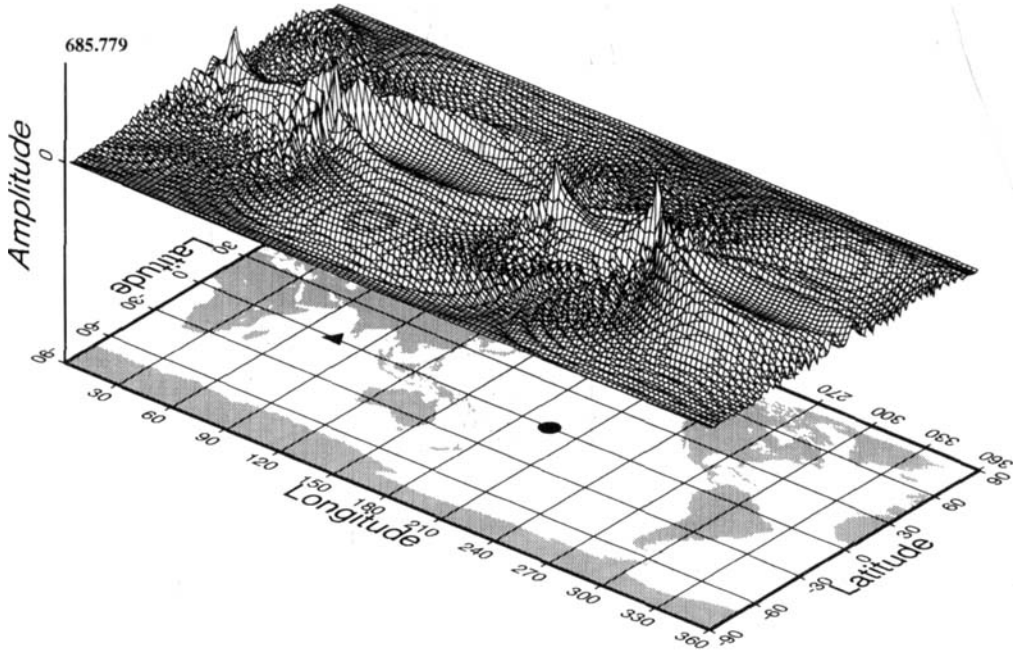

(d) *Frechet derivative kernel (model M84) : phase - time=6h*
multiplet 0S52 : isolated
perturbation in μ (0.1%) - double-couple source / vertical instrument

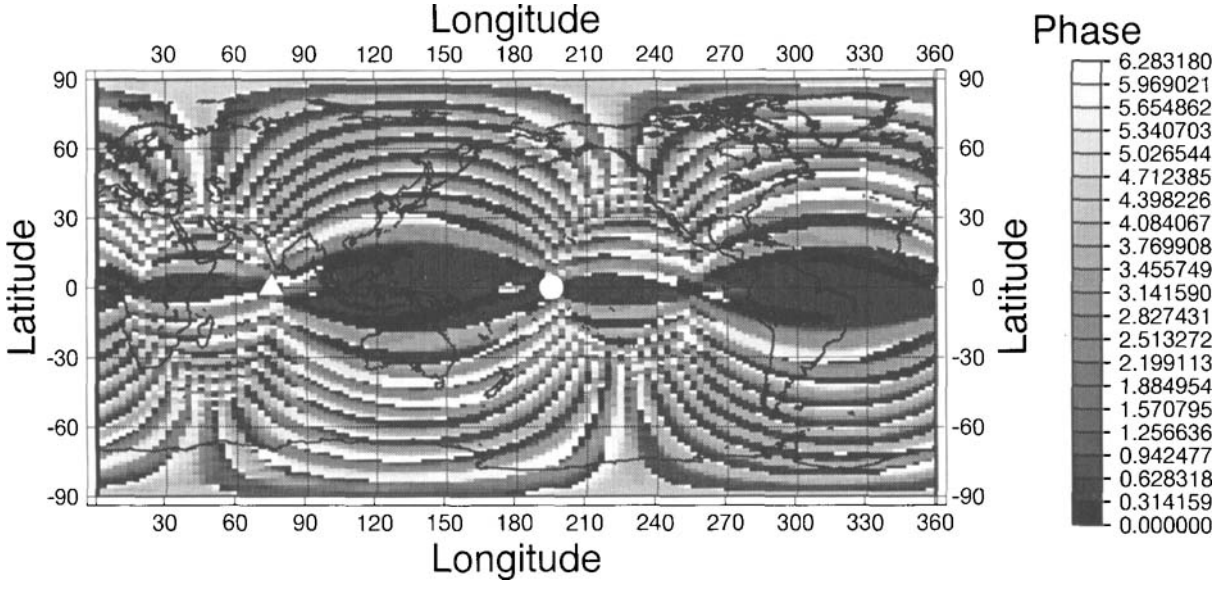

Figure 5. (*Continued*)

(e) *Frechet derivative kernel (model M84) : amplitude - time=12h*
multiplet 0S52 : isolated
perturbation in μ (0.1%) - double-couple source / vertical instrument

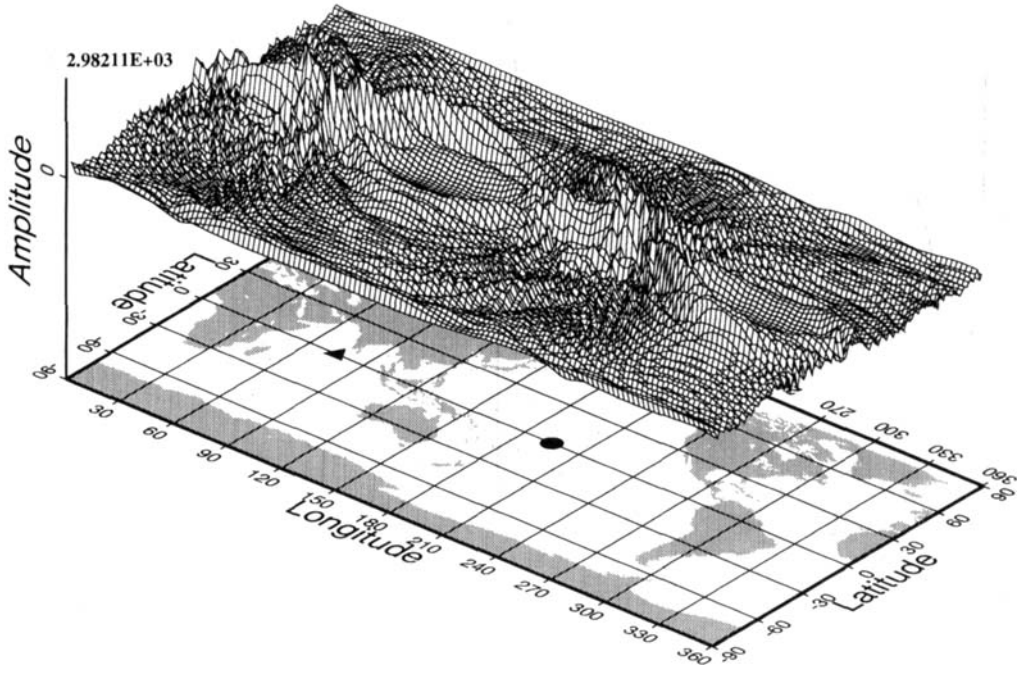

(f) *Frechet derivative kernel (model M84) : phase - time=12h*
multiplet 0S52 : isolated
perturbation in μ (0.1%) - double-couple source / vertical instrument

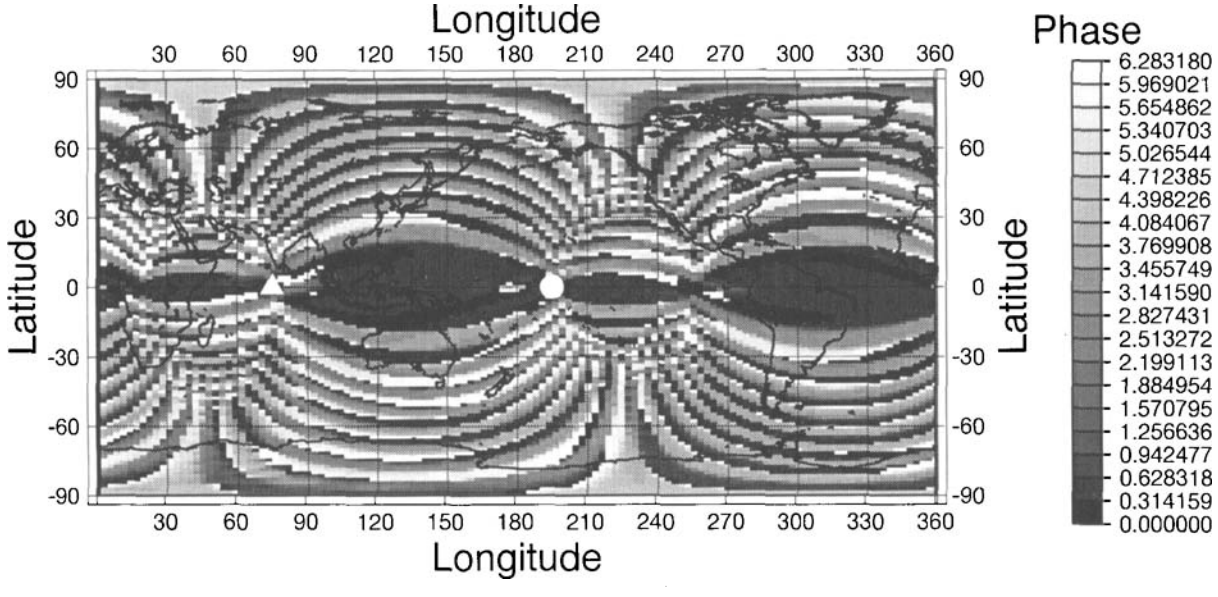

Figure 5. (*Continued*)

(a) *Frechet derivative kernel (model M84) : amplitude - time=0h*
multiplet 0S52 (coupling along the dispersion branch : +-3l)
perturbation in μ (0.1%) - double-couple source / vertical instrument

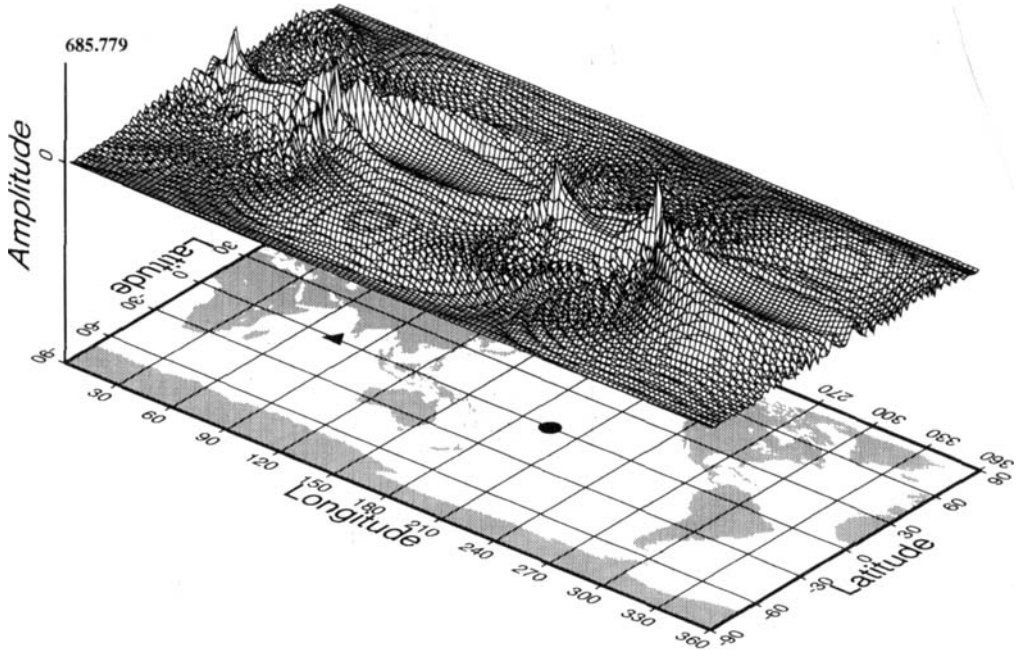

(b) *Frechet derivative kernel (model M84) : phase - time=0h*
multiplet 0S52 (coupling along the dispersion branch : +-3l)
perturbation in μ (0.1%) - double-couple source / vertical instrument

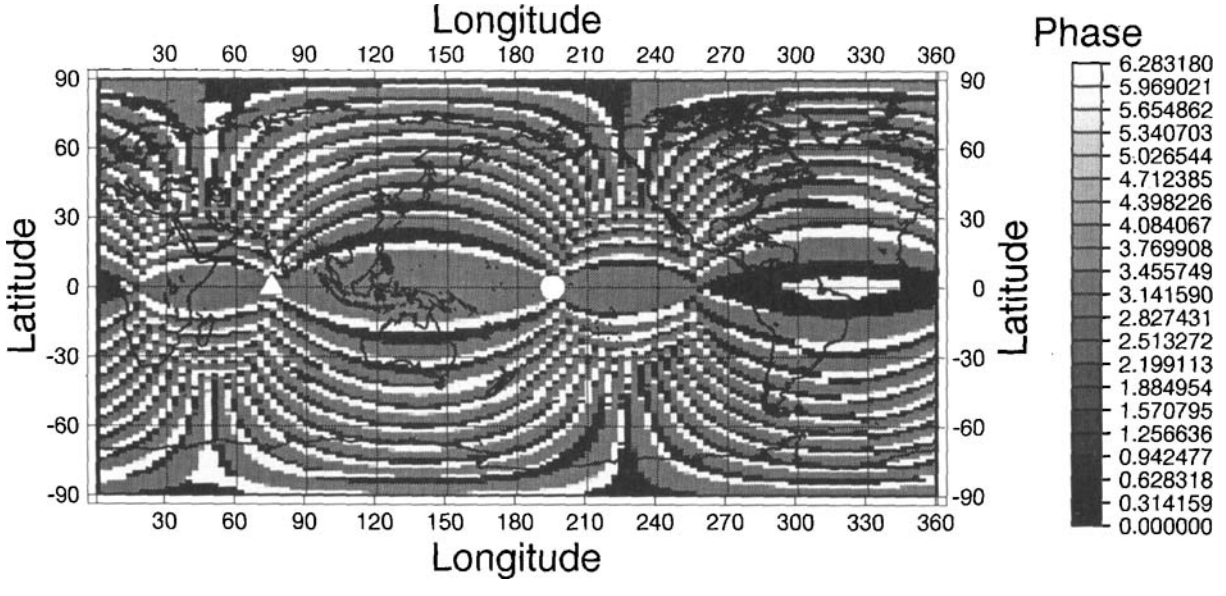

Figure 6. Coupled multiplets hypothesis: evolution of the Fréchet derivatives kernel (double-couple source) for ${}_0S_{52}$ for a perturbation in the shear modulus at several instants. The multiplet coupling is done for the six nearest modes around ${}_0S_{52}$ on the fundamental dispersion branch. Conventions are the same as for Fig. 5. The source mechanism is also the same. Coupling effects clearly appear at short times. These effects are located near strong velocity gradient zones and affect both phase and amplitude. They decrease with time, as the secular terms corresponding to the isolated multiplet contribution increase. (e) ($t = 12$ hr) presents the same pattern as Fig. 5(e), the isolated multiplet case. Only the corresponding phase (f) still shows differences from the isolated case (Fig. 5f).

(c) *Frechet derivative kernel (model M84) : amplitude - time=6h*
multiplet 0S52 (coupling along the dispersion branch : +-31)
perturbation in μ (0.1%) - double-couple source / vertical instrument

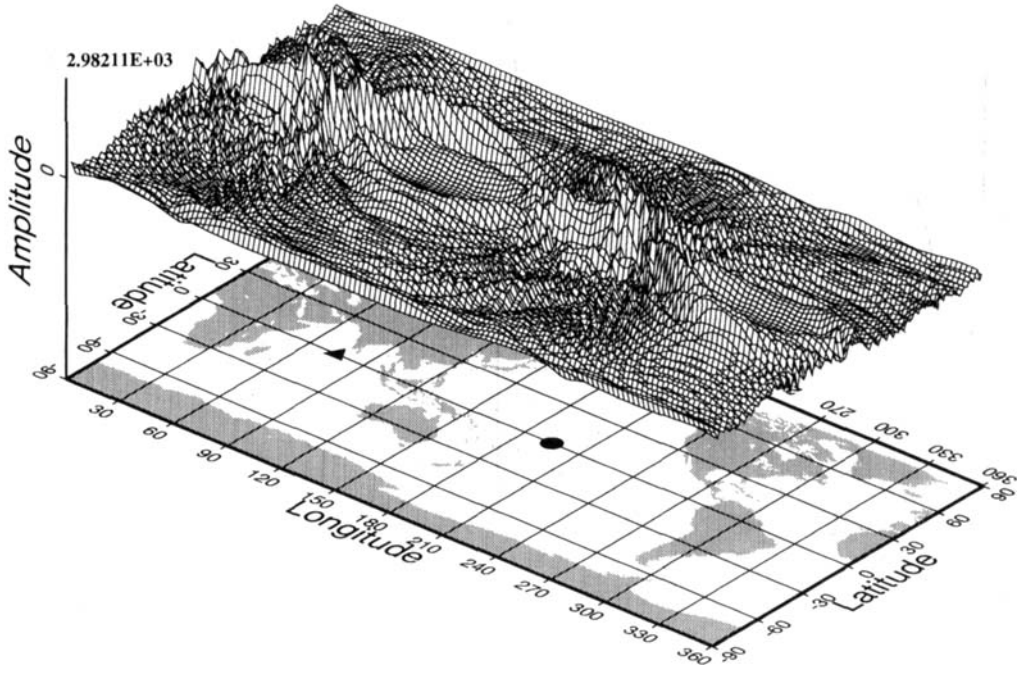

(d) *Frechet derivative kernel (model M84) : phase - time=6h*
multiplet 0S52 (coupling along the dispersion branch : +-31)
perturbation in μ (0.1%) - double-couple source / vertical instrument

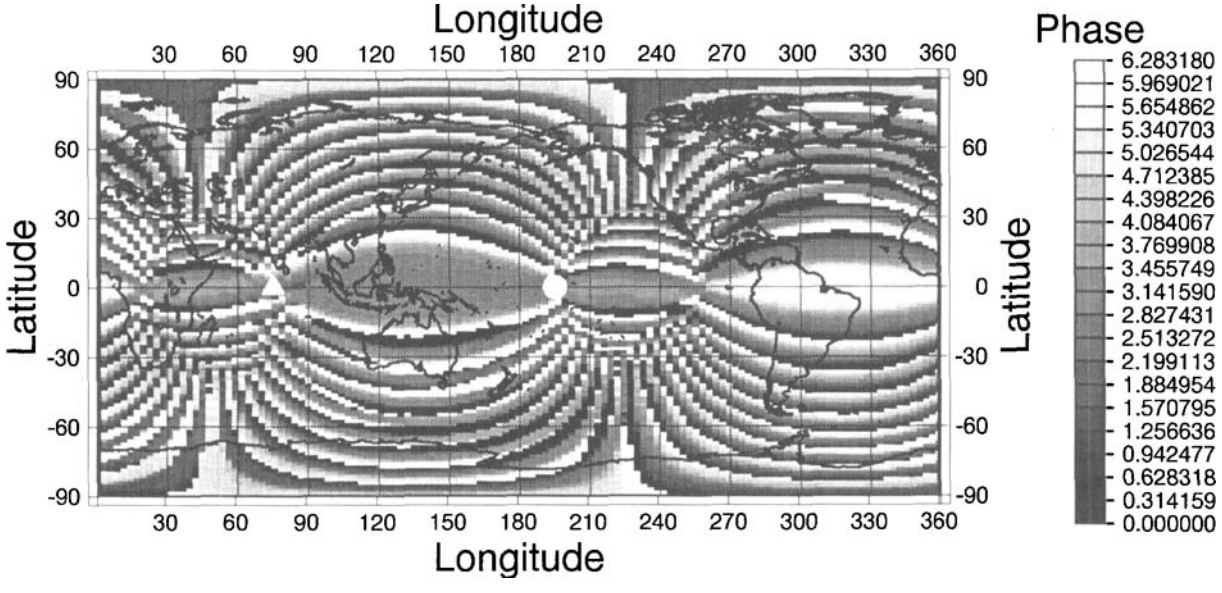

Figure 6. (*Continued*)

(e) *Frechet derivative kernel (model M84) : amplitude - time=12h*
multiplet 0S52 (coupling along the dispersion branch : +-3l)
perturbation in μ (0.1%) - double-couple source / vertical instrument

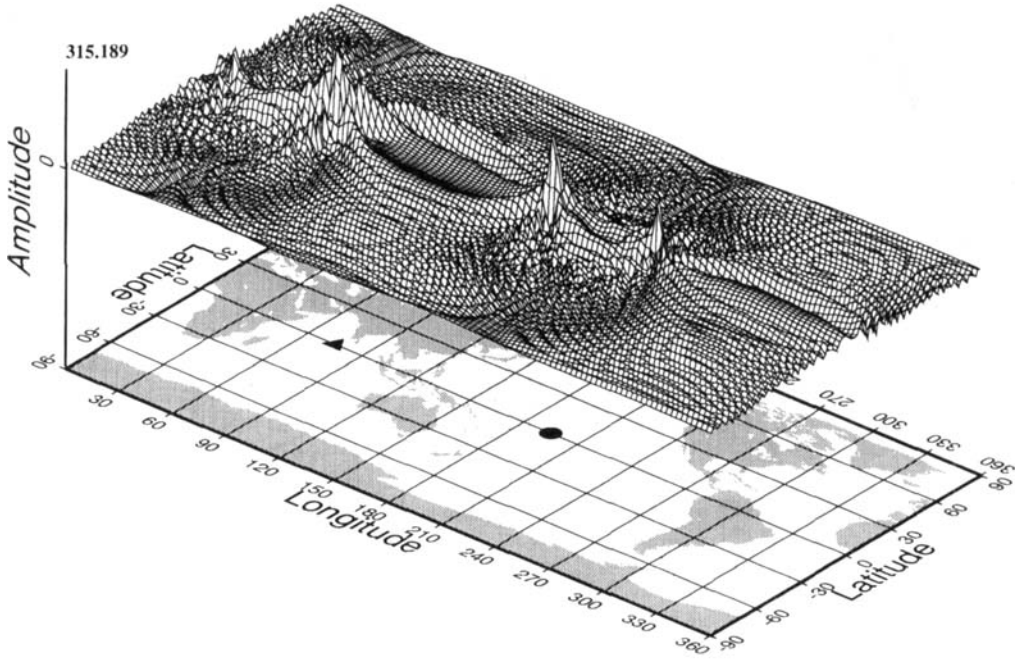

(f) *Frechet derivative kernel (model M84) : phase - time=12h*
multiplet 0S52 (coupling along the dispersion branch : +-3l)
perturbation in μ (0.1%) - double-couple source / vertical instrument

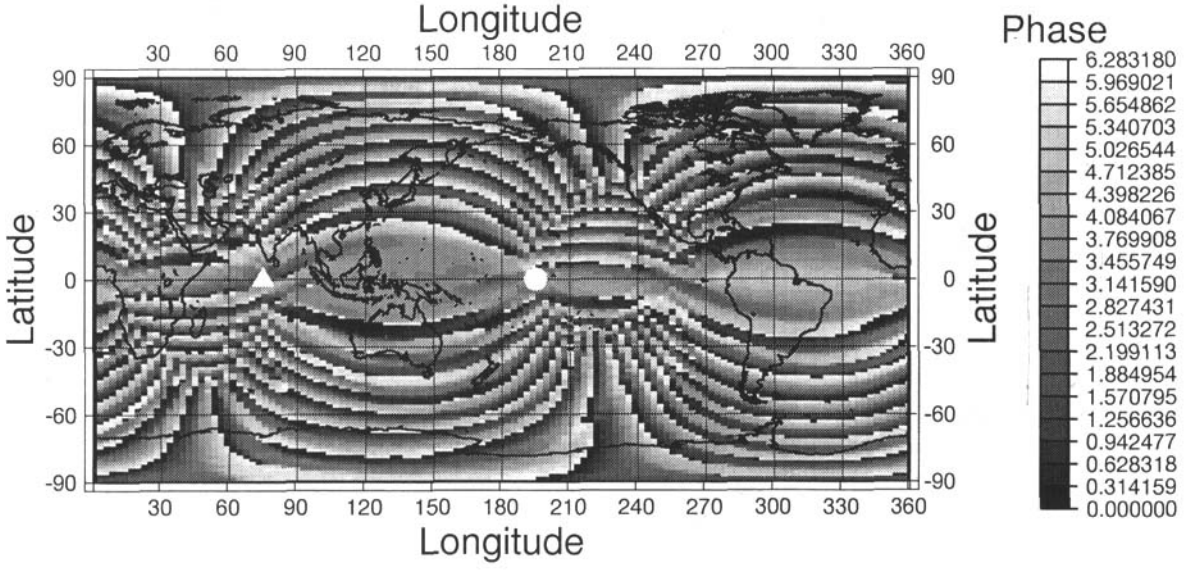

Figure 6. (*Continued*)

fact that the equatorial peak is very broad, and the sides lobes do not vanish toward the poles. Note that, at $t = 0$, the kernel is a purely real quantity, all modulation fields being purely real (there is no aspherical attenuation in our model). As time increases, the maximum of energy moves slowly from its initial location to reach an orbit corresponding to the most excited singlets for the source–receiver couple (Figs 5c and e), while the kernel becomes fully complex. The spherical great-circle approximation is no longer valid; indeed, our Fréchet derivative kernel appears to be essentially sensitive to the structure beneath a path which is not exactly the geometrical great circle, and which slowly precesses with time. We now look at the terms in the Fréchet derivative [given by (39)] involving coupling along a particular dispersion branch. Figs 6(a)–(f) show the kernels for the same time as in Figs 5(a)–(f). The summation in (39) is only done for the six closest modes along the dispersion branch.

If self-coupling gives sensitivity to even degree structure, coupling along the branch introduces asymmetries (odd structure) between major and minor arcs and allows us to see focusing effects (e.g. Romanowicz 1987). Indeed, at $t = 0$, the departure from the spherical case is greater than previously. We observe strong focusing effects near strong velocity gradient zones, thus showing that the path-average approximation is no longer valid. Sensitivity along the R_1 path is different from the sensitivity along the R_2 path. However, as the self-coupling part is a secular term, with an amplitude that increases fairly linearly with time, the relative importance of the coupling terms with respect to the self-coupled terms will vary as

$$\frac{\text{coupled}}{\text{isolated}} \simeq \frac{1}{(\sigma_K - \sigma_{K'})t},$$

where t is the time. In our example, at time $t = 4$ hr, the typical contribution of the coupling effect is more than 50 per cent of the total amplitude. This contribution is the only one that is significantly sensitive to the lateral heterogeneities with odd-order symmetry. Indeed, the self-coupling part, due to the selection rules, is mostly sensitive to the even part of lateral heterogeneities even though, in contrast to the case of the Fréchet derivative with respect to a spherical earth, it has a small sensitivity to the odd part (Woodhouse 1983; Romanowicz 1987; Park 1987). As a consequence, the sensitivity of the complete Fréchet derivative to lateral variations with odd-order symmetry decreases as time increases. This is especially true for inversions based on resolved normal modes, which need a long time series (Ritzwoller *et al.* 1986, 1988; Giardini *et al.* 1987, 1988). If we want to use a single resonant peak, it is necessary to separate modes with frequency differences of $(\sigma_K - \sigma_{K'})$, and the length of the series must then be such that

$$(\sigma_K - \sigma_{K'})t > 1.$$

The Fréchet derivative is then dominated by the self-coupling secular term, and therefore mainly sensitive to the even-order lateral variations, confirming numerical results shown by Hara *et al.* (1993).

We have also computed the Fréchet derivative kernels for the low-angular-order mode ${}_0S_{17}$. The computation has been performed using the same receiver and double-couple source as for ${}_0S_{52}$. Figs 7(a)–(f) shows the Fréchet derivative kernel for a perturbation of 0.1 per cent in μ, at the initial time (Figs 7a and b), after 24 hr (Figs 7c and d) and after 48 hr (Figs 7e and f). The same features as previously appear, but here secondary side lobes around the main path are very important, due to the rather low angular order of the mode ${}_0S_{17}$. After 48 hr, the main contribution to the amplitude comes from the secular terms corresponding to the self-coupling part.

Considering Fréchet derivative kernels computed for an isotropic source, the comparison with the results obtained with the vertical strike-slip source shows that the amplitude pattern appears to be fairly independent of the mechanism of the source, except near the source location. The difference is in the phase values, where in our case a quasi-constant π dephasing occurs between the kernels obtained with the two different types of mechanism.

5.3 Local frequency and comparison between elastic/anelastic perturbations

Let us compare our results in the context of local frequency, and try to address the problem of attenuation sensitivity to effects of focusing/defocusing (Levshin, Ritzwoller & Ratnikova 1994; Romanowicz 1994). We can define the local frequency associated with a modulation function as

$$A_K(t) = A_K(0) \exp[it\delta\sigma(t)],$$

so that the perturbation of the local frequency, for short time, is given by

$$d\delta\sigma_K(t) \simeq \frac{1}{it}\left[\frac{dA_K}{A_K(t)} - \frac{dA_K(0)}{A_K(0)}\right]. \quad (42)$$

A real perturbation of the local frequency may be, to the first order, and without focusing/defocusing corrections, associated with a real perturbation of the stiffness tensor, while an imaginary perturbation of the local frequency may be associated with the imaginary part. The map of the perturbation of the local frequency of ${}_0S_{52}$ is shown in Figs 8(a)–(d). The amplitude of the real and imaginary parts along the equatorial path is shown in Figs 9(a)–(b) and 10(a)–(b), 2 and 4 hr after the earthquake for perturbations in μ and Q_μ, respectively.

Figs 9(a)–(b) show the predominance of a real perturbation of the local frequency for a real perturbation of the stiffness tensor over most of the R_1 and R_2 paths, except between the antipode of the source and the receiver, where focusing is strong and where both the real and imaginary parts have terms of equal amplitude.

In contrast, for imaginary perturbations of the stiffness tensor (Fig. 10a–b) we end up with a less pronounced signature on the local frequency: the real perturbation is at least half of the imaginary one, and is even predominant between the antipode of the source and the receiver.

In all cases, we have a strong focusing of the sensitivity near the location of the source, receiver, and their antipodes by a factor of 3 to 5. Note that the imaginary perturbation of the local frequency, which appears for a 1 per cent lateral variation in the shear modulus, is roughly equivalent in amplitude to the signal associated with a 5 per cent lateral variation in the imaginary part of the shear modulus.

6 SYNTHETIC FOURIER SPECTRUM

The theoretical results given in Sections 1–4, and illustrated in Section 5, enable a theoretical seismogram and its partial

(a) *Frechet derivative kernel (model M84) : amplitude - time=0h*
multiplet 0S17 (coupling along the dispersion branch +-3l)
perturbation in μ (0.1%) - double-couple source / vertical instrument

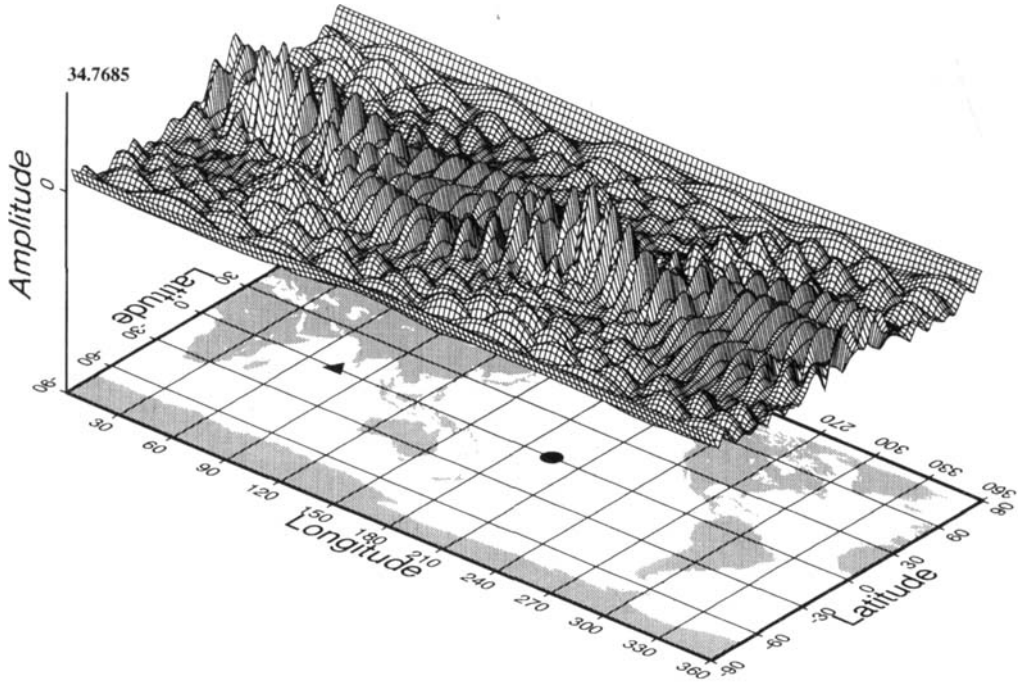

(b) *Frechet derivative kernel (model M84) : phase - time=0h*
multiplet 0S17 (coupling along the dispersion branch +-3l)
perturbation in μ (0.1%) - double-couple source / vertical instrument

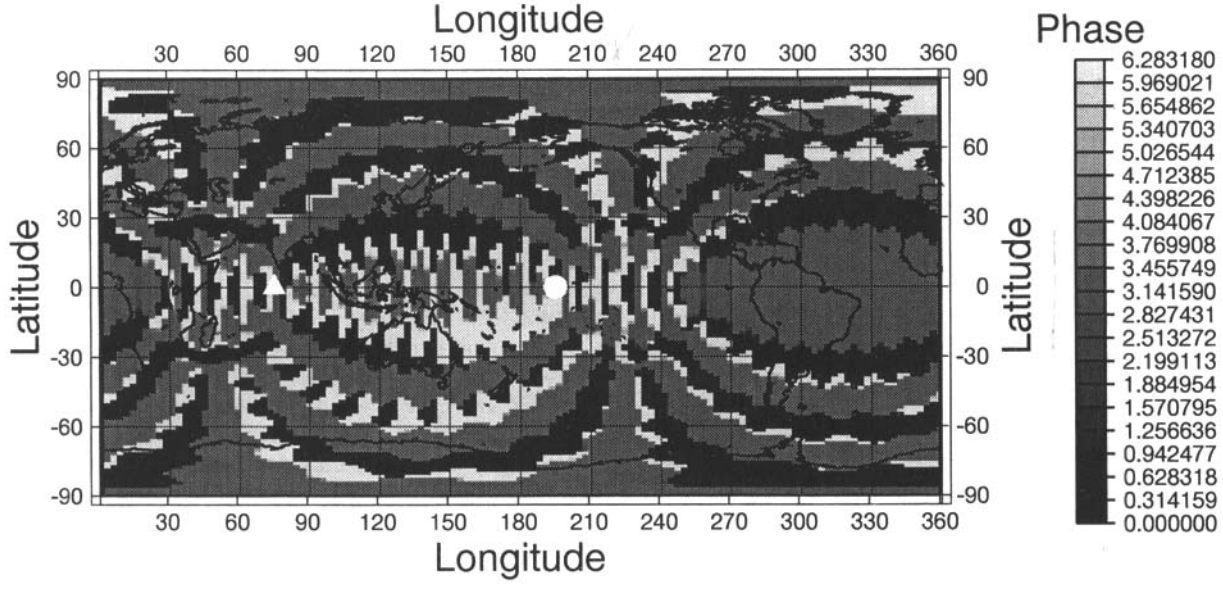

Figure 7. Coupled-multiplet hypothesis: evolution of the Fréchet derivatives kernel for ${}_0S_{17}$ (double-couple source) for a perturbation in μ (0.1 per cent). Conventions are as in Figs 5 and 6. (a) and (b) show, respectively, the amplitude and phase at the initial time. The Fréchet derivative kernels in amplitude and phase are given after 24 hr in (c) and (d), and after 48 hr in (e) and (f).

(c) *Frechet derivative kernel (model M84) : amplitude - time=24h*
multiplet 0S17 (coupling along the dispersion branch +-3l)
perturbation in μ (0.1%) - double-couple source / vertical instrument

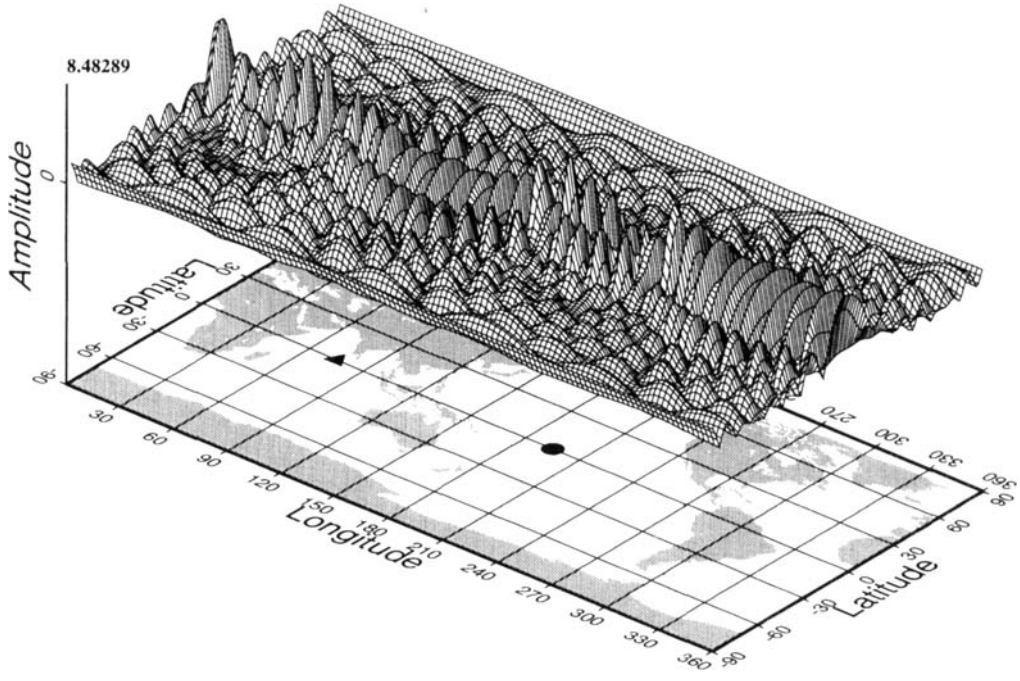

(d) *Frechet derivative kernel (model M84) : phase - time=24h*
multiplet 0S17 (coupling along the dispersion branch +-3l)
perturbation in μ (0.1%) - double-couple source / vertical instrument

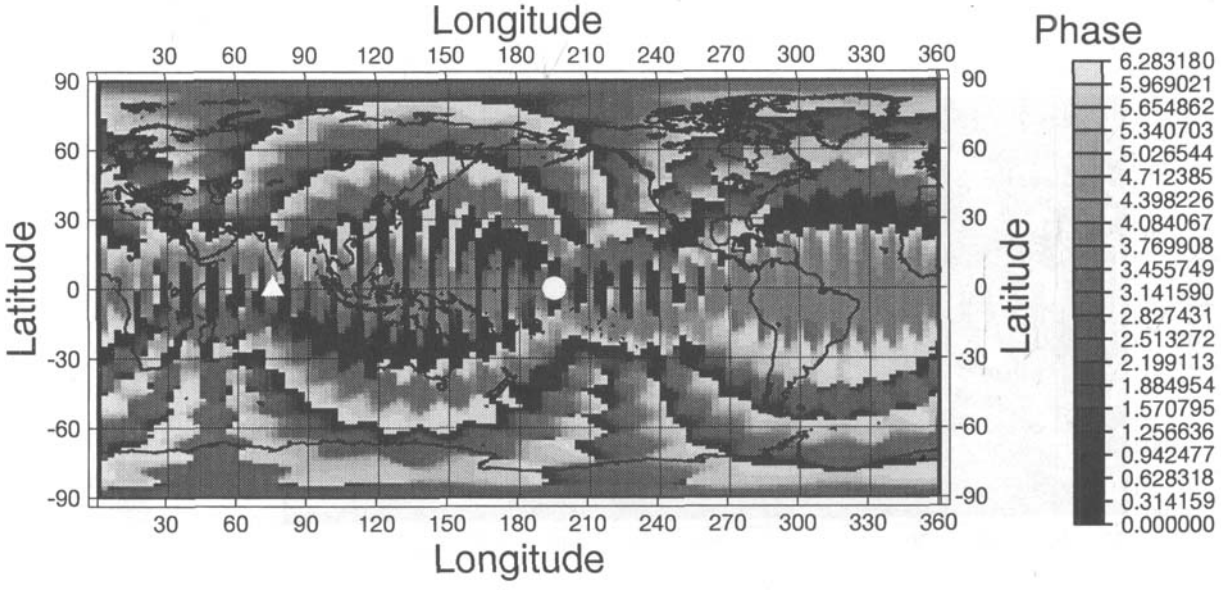

Figure 7. (*Continued*)

(e) *Frechet derivative kernel (model M84) : amplitude - time=48h*
multiplet 0S17 (coupling along the dispersion branch +-31)
perturbation in μ (0.1%) - double-couple source / vertical instrument

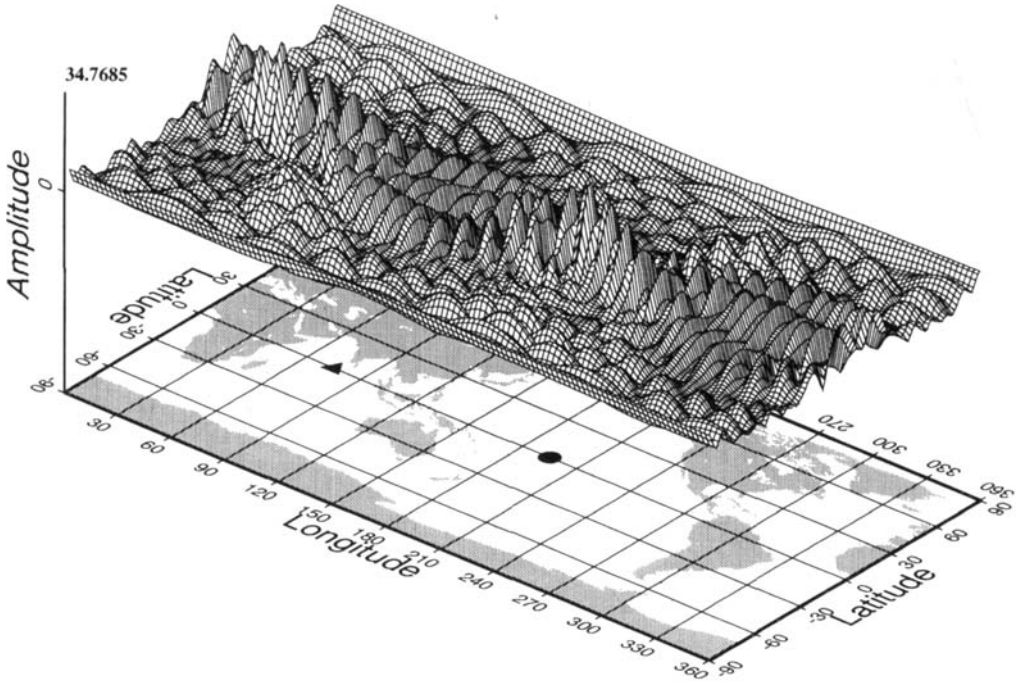

(f) *Frechet derivative kernel (model M84) : phase - time=48h*
multiplet 0S17 (coupling along the dispersion branch +-31)
perturbation in μ (0.1%) - double-couple source / vertical instrument

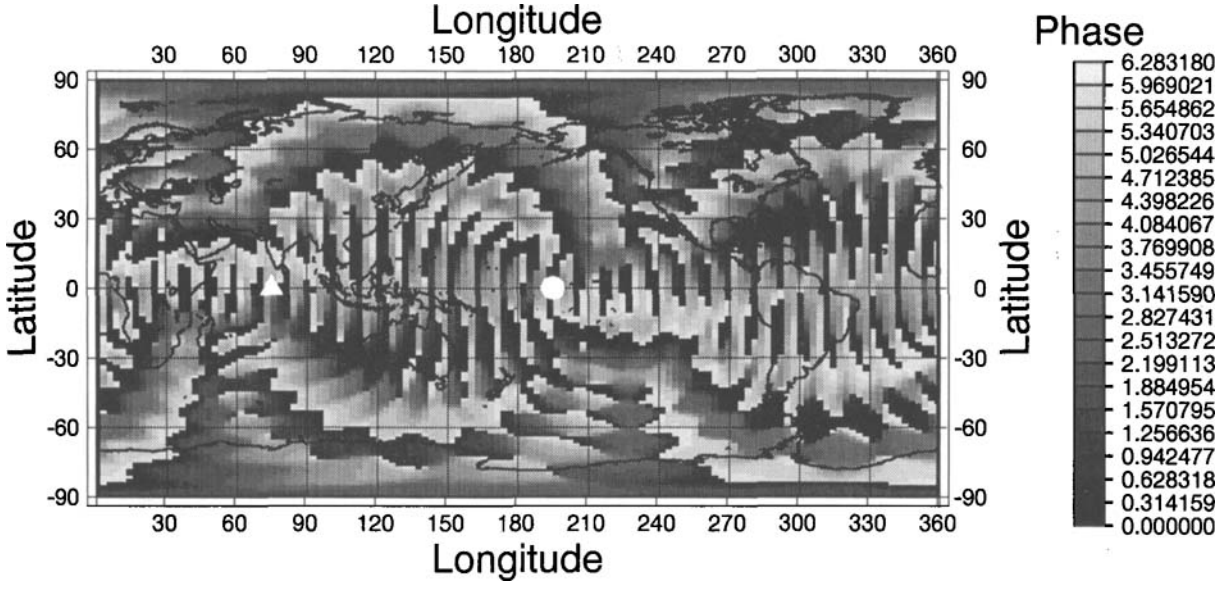

Figure 7. (*Continued*)

(a) *Perturbation of the instantaneous frequency (model M84) : real part - time=2h*
multiplet 0S52 (coupling along the dispersion branch : +-3l)
perturbation in μ (0.1%) - double-couple source / vertical instrument

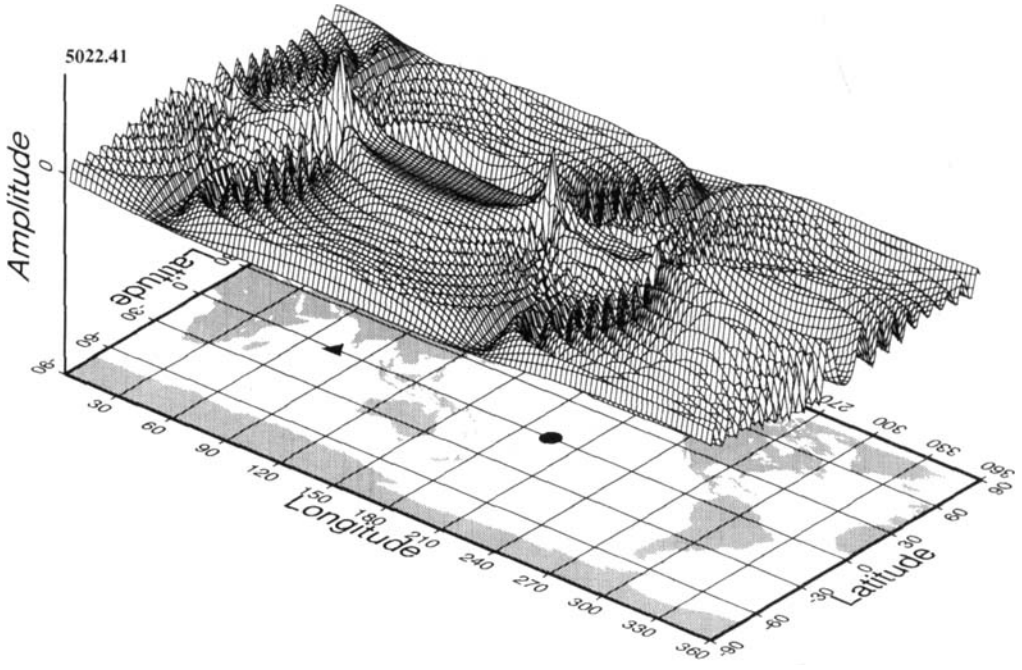

(b) *Perturbation of the instantaneous frequency (model M84) : imaginary part - time=2h*
multiplet 0S52 (coupling along the dispersion branch : +-3l)
perturbation in μ (0.1%) - double-couple source / vertical instrument

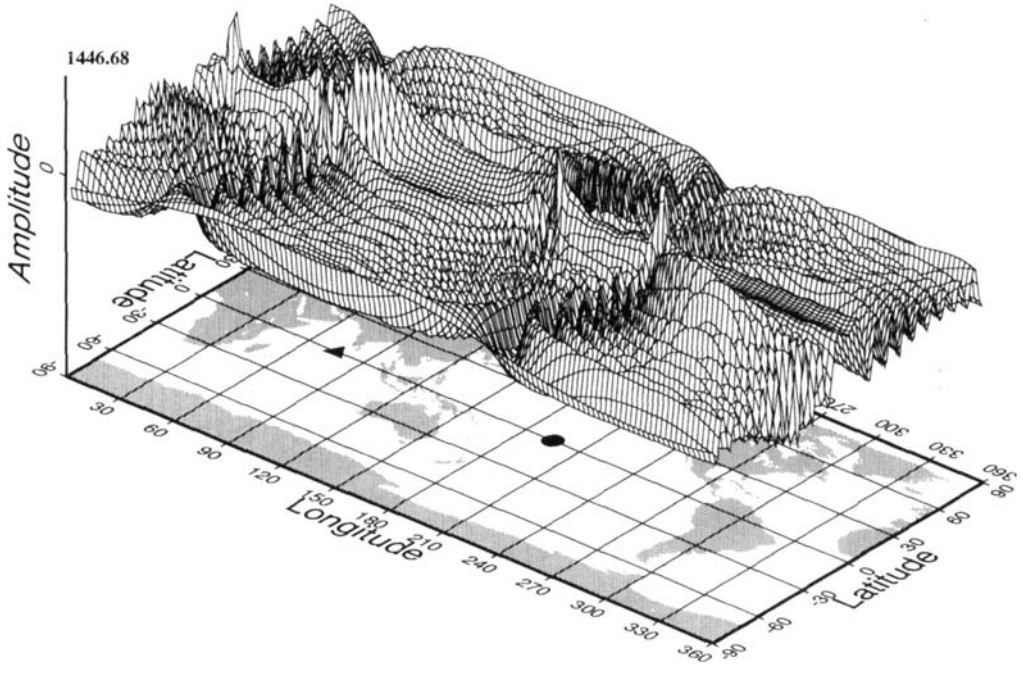

Figure 8. Perturbation of the local eigenfrequency of the multiplet ${}_0S_{52}$. These maps show the perturbation of the local frequency, as defined by the relation (42). Conventions are as in Figs 5 to 7. (a) and (b) show the real and imaginary parts of the frequency (depth is 500 km) due to a local variation of the shear modulus of 1 per cent at time $t = 2$ hr, while (c) and (d) give the field induced by a local variation of the attenuation factor Q_μ of 10 per cent at the same time. These two kinds of perturbation yield the same order of magnitude for the perturbation of the complex frequency.

(c) *Perturbation of the instantaneous frequency (model M84) : real part - time=2h multiplet 0S52 (coupling along the dispersion branch : +-3l) perturbation in Q_μ (10%) - double-couple source / vertical instrument*

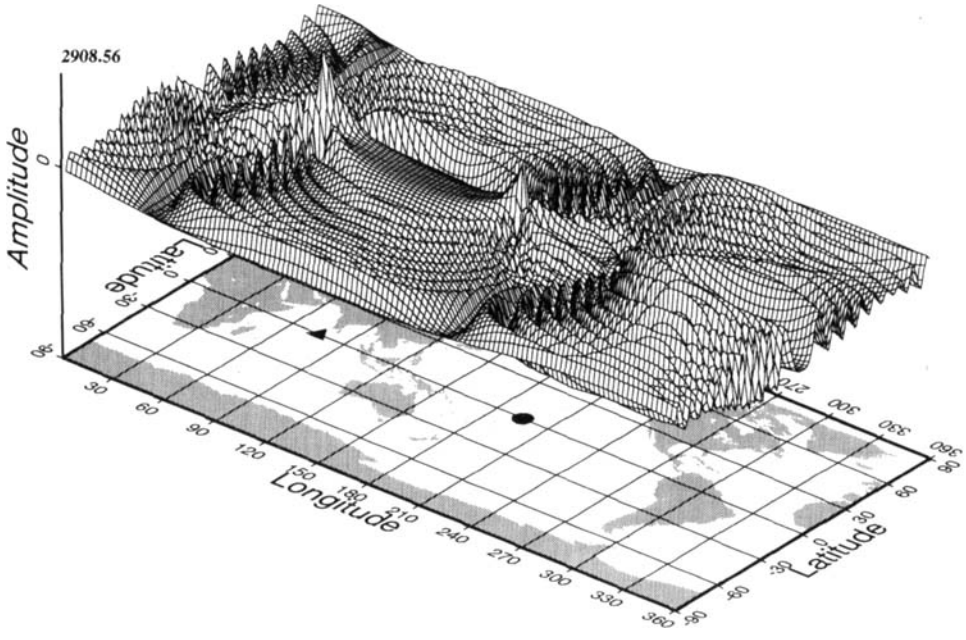

(d) *Perturbation of the instantaneous frequency (model M84) : imaginary part - time=2h multiplet 0S52 (coupling along the dispersion branch : +-3l) perturbation in Q_μ (10%) - double-couple source / vertical instrument*

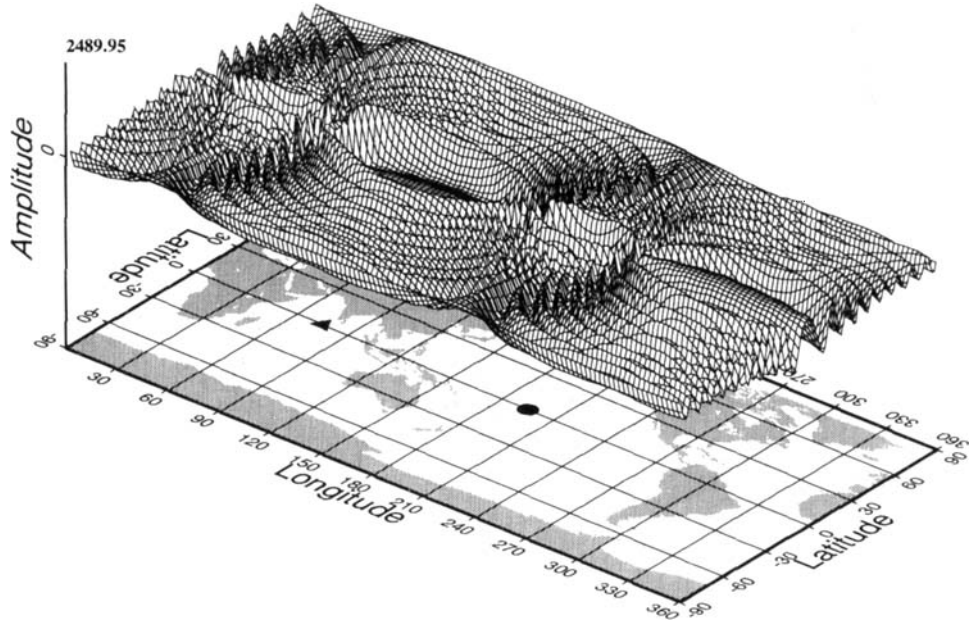

Figure 8. (*Continued*)

(a) Perturbation of the instantaneous complex frequency of the multiplet 0S52 along the equator
perturbation in shear modulus (0.1%), time=2h, source: double couple, depth=500kms

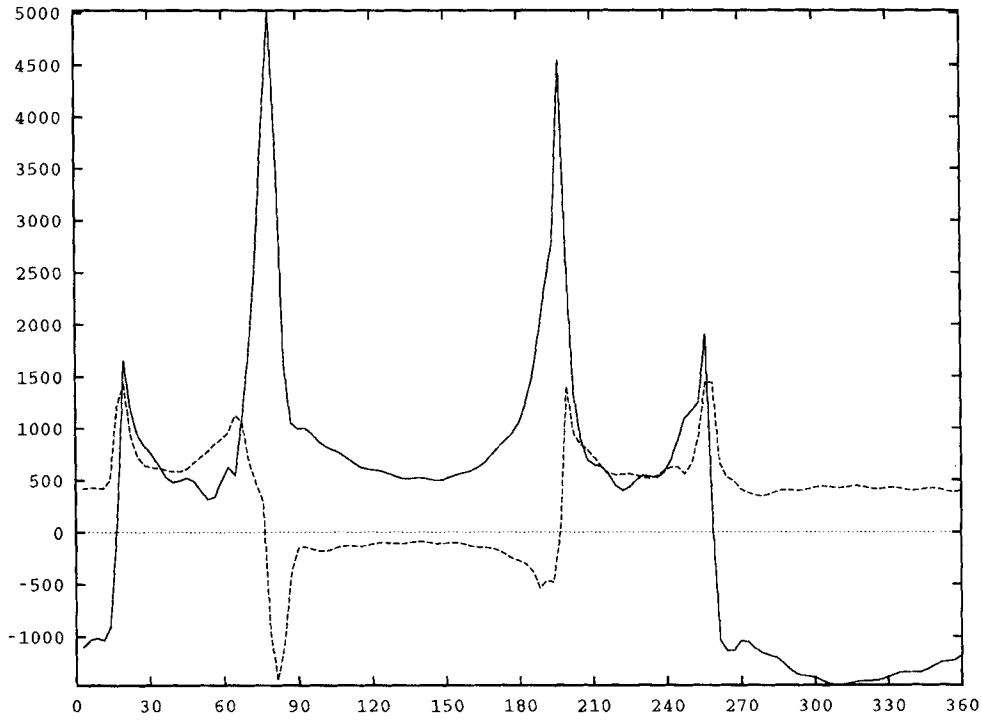

(b) Perturbation of the instantaneous complex frequency of the multiplet 0S52 along the equator
perturbation in shear modulus (0.1%), time=4h, source: double couple, depth=500kms

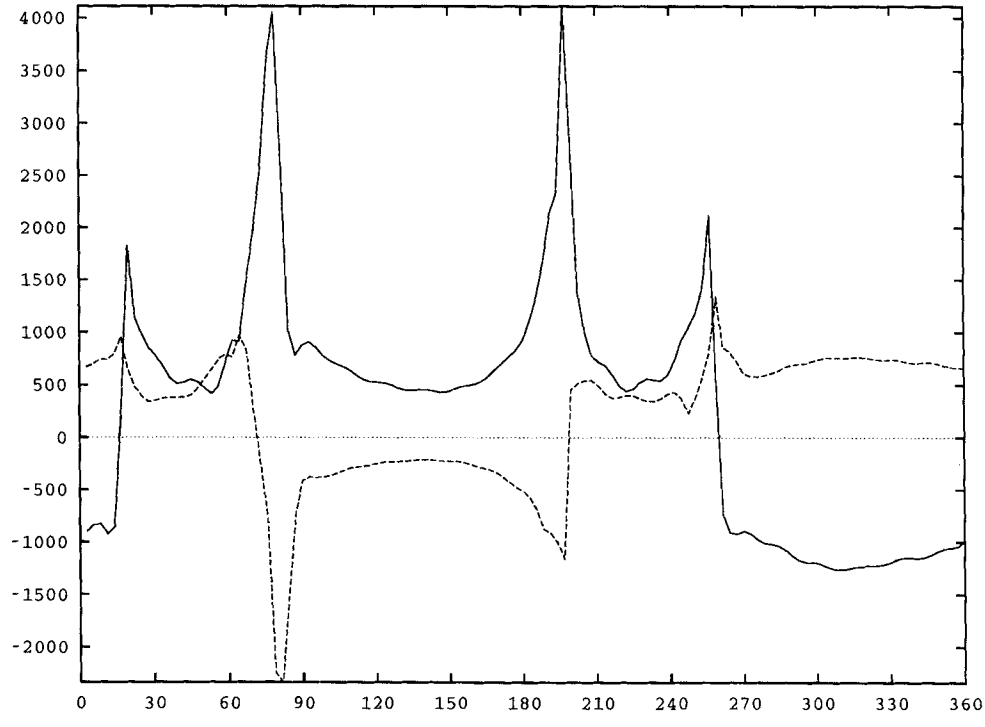

Figure 9. Perturbation of the local eigenfrequency of the multiplet ${}_0S_{52}$ along the equator for a perturbation in μ (0.1 per cent). The perturbation is taken along the geometrical great circle, for time $t = 2$ hr in (a) (extracted from Figs 8a and b), and for time $t = 4$ hr in (b). The continuous curves represent the real parts of the perturbations, corresponding to apparent phase perturbations, while the dashed lines are for the imaginary parts, producing focusing/defocusing effects or attenuation effects. The real perturbation of the local frequency is predominant for most of the R_1 and R_2 paths. In contrast, the loci of strong focusing show an equal contribution to the real and imaginary parts of the local frequency perturbation.

(a) Perturbation of the instantaneous complex frequency of the multiplet 0S52 along the equator

perturbation in Q-shear (10%), time=2h, source: double-couple, depth=500kms

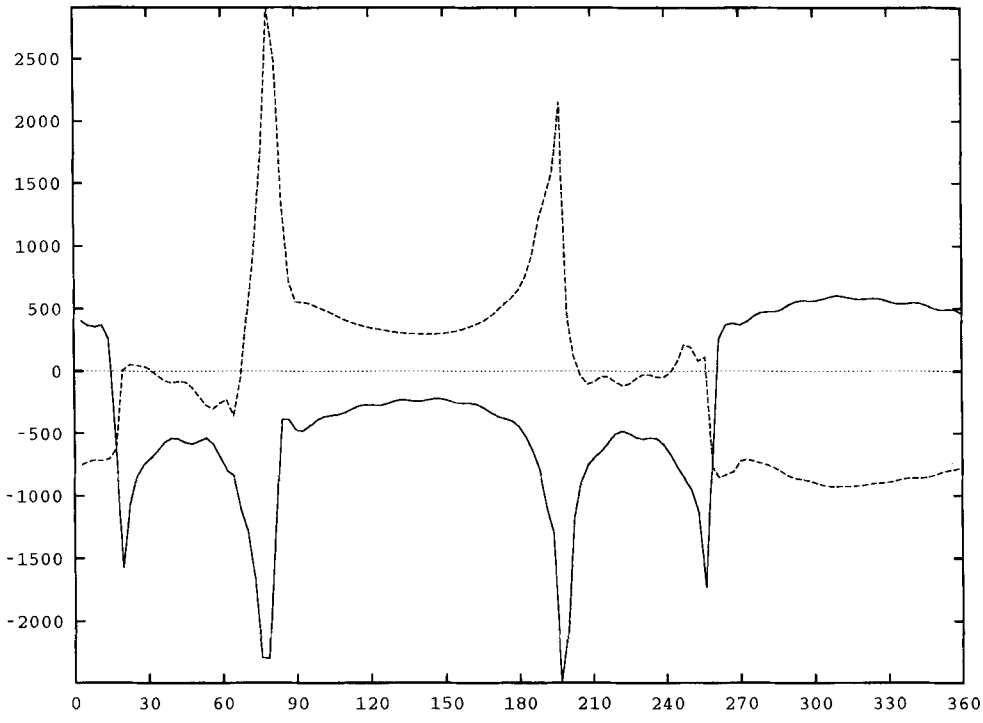

(b) Perturbation of the instantaneous complex frequency of the multiplet 0S52 along the equator

perturbation in Q-shear (10%), time=4h, source: double-couple, depth=500kms

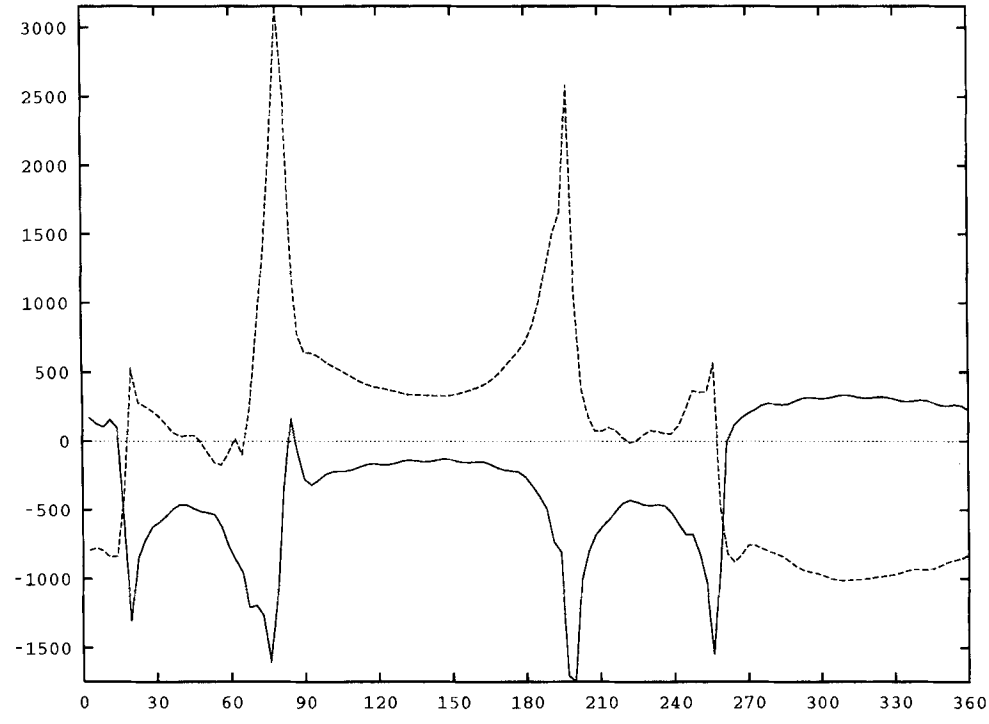

Figure 10. Perturbation of the local eigenfrequency of the multiplet ${}_0S_{52}$ along the equator for a perturbation in Q_μ (10 per cent). Conventions are the same as for Fig. 9. (a) is extracted from Figs 8(b) and (c). In this case, the real part of the local frequency perturbation becomes predominant along the shortest paths between the source and receiver locations and their antipodes. Note that a 5 per cent lateral variation in the imaginary part of the shear modulus gives a roughly equivalent amplitude of the local frequency perturbation to that obtained with a 1 per cent lateral variation in the real part of the shear modulus.

derivatives to be calculated. In the same way, we can obtain synthetic spectra through the modulation function formalism.

Nowab & Lognonné (1994) show that for a synthetic seismogram expressed as

$$s(t) = \sum_K \mathscr{R}e[\exp(i\sigma_K t) A_K(t)], \tag{43}$$

with, following eqs (10) and (12),

$$A_K(t) = \langle \mathbf{R} | \mathbf{S}_K(t) \rangle = \langle \mathbf{R}_K(t) | \mathbf{S} \rangle, \tag{44}$$

the corresponding Fourier spectrum can be obtained analytically.

If $s(t)$ is cut into N segments $[T_n, T_{n+1}]$ of length ΔT, its Fourier transform can be written as

$$s(\omega) = \sum_K \sum_{n=1}^{N} s_K^n(\omega), \tag{45}$$

with

$$s_K^n(\omega) = \sum_{t_{1n}}^{t_{2n}} A_K(t) \exp[i(\sigma_K - \omega)t]\, \delta t, \tag{46}$$

where δt represents the time spacing between data points in the initial time series, and t_{1n} and t_{2n} are respectively the times for the first and last points in the nth segment.

As shown by Nawab & Lognonné (1994), the modulation function $A_K(t)$ can be modelled by a cubic polynomial over each nth segment. This leads to the analytical expression for the Fourier spectrum:

$$\begin{aligned} s(\omega) = \sum_K \sum_{n=1}^{N} & \exp[i(\sigma_K - \omega)t_{1n}] \\ & \times [A_K(T_n) d_1^n(\omega) + A_K(T_{n+1}) d_2^n(\omega) \\ & + \dot{A}_K(T_n) \Delta T d_3^n(\omega) + \dot{A}_K(T_{n+1}) \Delta T d_4^n(\omega)]\, \delta t, \end{aligned} \tag{47}$$

where $\dot{A}_K$ represents the time derivative of A_K, and where the functions $d_1^n(\omega)$, $d_2^n(\omega)$, $d_3^n(\omega)$ and $d_4^n(\omega)$ depend only on the spherical frequency of the multiplet and on the number of points per sequence. Expressions for these functions are detailed in Nawab & Lognonné (1994). In the same way, the Fréchet derivatives of the spectrum can be calculated using expression (47), by replacing the modulation functions by their Fréchet derivatives.

7 CONCLUSION

We have formulated expressions for Fréchet derivative seismograms for elastic, anelastic and physical dispersion perturbations in a laterally heterogeneous earth model. These results are based on the concept of modulation fields considered independently, either at the sources or at the receivers. These fields condense all the effects on seismograms produced by lateral variations of the Earth. They are characterized by slow modulations in time, involving a characteristic time-scale comparable to the inverse of the frequency splitting width and not to the period of the mode. Moreover, the computation of $N \times M$ seismograms and their related Fréchet derivatives only requires the computation of M source modulation functions and N receiver modulation functions.

In order to compute the modulation fields rapidly, a 'direct solution' technique has been proposed which avoids the computation of the aspherical normal modes. This technique is based on perturbation theory, expressed up to the second order for amplitudes, and up to the third order for frequencies, using the results of Lognonné (1991). Thus the time-varying modulation functions use the aspherical normal modes implicitly, but need explicitly only the SNRAI spherical harmonic normal modes and coupling matrices. Hence, the Fréchet derivatives of the seismograms can be rapidly computed for every point of an aspherical anelastic 3-D earth.

The numerical tests performed show some large differences from the spherical symmetric case. First, the frozen-path approximation is no longer valid since the sensitivity of the seismogram shifts with time from the initial great-circle path. The path 'selected' depends both on the source and receiver characteristics, and on the structure. Secondly, focusing effects due to the coupling of the closest modes along a single dispersion branch invalidate the use of a great-circle path average to retrieve the structure. The importance of these coupling effects at small times cannot be neglected, and otherwise may result in a wrong localization of the lateral heterogeneities.

Direct inversion of the structural information carried by the modulation functions is already possible (Nawab 1993), as these secondary observables can now be well determined using, for example, the normal-mode demodulation technique proposed by Nawab & Lognonné (1994). The theoretical formulation given here is a first step to global inversion of seismic waveforms. The fast computation of synthetic seismograms through the modulation field approach and the Fréchet derivatives of these seismograms with respect to the structural parameters, as well as the fact that the algorithm derived from this formulation is well adapted to parallel computers, make this kind of inversion feasible.

ACKNOWLEDGMENTS

We thank B. Romanowicz and A. Forte for reading this paper and making helpful comments. We also thank J.-P. Montagner for profitable discussions. This research was supported by CNRS/INSU under ATP Tomographie and by CNCPST/IDRIS under contract J00015. This is IPGP contribution 1394.

REFERENCES

Dalhen, F.A., 1974. Inference of the lateral heterogeneities of the Earth from the eigenfrequency spectrum: a linear inverse problem, *Geophys. J. R. astr. Soc.*, **38**, 143–167.

Dalhen, F.A. & Henson, I.H., 1985. Asymptotic normal modes of laterally heterogeneous Earth, *J. geophys. Res.*, **90**, 12 653–12 681.

Dziewonski, A.M. & Anderson, D.L., 1981. Preliminary Reference Earth Model, *Phys. Earth planet. Inter.*, **25**, 297–356.

Geller, R.J. & Hara, T., 1993. Two efficient algorithms for iterative linearized inversion of seismic waveform data, *Geophys. J. Int.*, **115**, 699–710.

Giardini, D., Li, X.-D. & Woodhouse, J.H., 1987. Three-dimensional structure of the Earth from splitting in free oscillation spectra, *Nature*, **325**, 405–411.

Giardini, D., Li, X.-D. & Woodhouse, J.H., 1988. Splitting functions of long-period normal modes of the Earth, *J. geophys. Res.*, **93**, 13 716–13 742.

Hara, T., Tsuboi, S. & Geller, R.J., 1991. Inversion for laterally heterogeneous earth structure using laterally heterogeneous starting model: preliminary results, *Geophys. J. Int.*, **104,** 523–540.

Hara, T., Tsuboi, S. & Geller, R.J., 1993. Inversion for laterally heterogeneous upper mantle *S*-wave velocity structure using iterative waveform inversion, *Geophys. J. Int.*, **115,** 667–698.

Henson, I.H. & Dalhen, F.A., 1986. Asymptotic normal modes of laterally heterogeneous Earth. 2. Further results, *J. geophys. Res.*, **91,** 12 467–12 481.

Jordan, T.H., 1978. A procedure for estimating lateral variations from low-frequency eigenspectra data, *Geophys. J. R. astr. Soc.*, **52,** 441–455.

Levshin, A.L., Ritzwoller, M.H. & Ratnikova, L.I., 1994. The nature and cause of polarization anomalies of surface waves crossing northern and central Asia, *Geophys. J. Int.*, **117,** 577–590.

Li, X.-D. & Romanowicz, B., 1995. Comparison of global waveform inversions with and without considering cross-branch modal coupling, *Geophys. J. Int.*, **121,** 695–709.

Liu, H.P., Anderson, D.L. & Kanamori, H., 1976. Velocity dispersion due to anelasticity; implications for seismology and mantle composition, *Geophys. J. R. astr. Soc.*, **47,** 41–58.

Lognonné, P., 1991. Normal modes and seismograms in an anelastic rotating Earth, *J. geophys. Res.*, **96,** 20 309–20 319.

Lognonné, P. & Romanowicz, B., 1990a. Effect of a global plume distribution on Earth normal modes, *Geophys. Res. Lett.*, **17,** 1493–1495.

Lognonné, P. & Romanowicz, B., 1990b. Fully coupled Earth's vibrations: the spectral method, *Geophys. J. Int.*, **102,** 365–395.

Nawab, R., 1993. Observation et démodulation des modes propres de la Terre: contraintes sur la Terre profonde, *PhD thesis,* University of Paris 7, Paris.

Nawab, R. & Lognonné, P., 1994. A new technique in normal modes demodulation, *Phys. Earth planet. Inter.*, **84,** 139–160.

Nolet, G., 1993. Imaging the upper mantle with partitioned non-linear waveform inversion, in Seismic tomography: theory and practice, pp. 248–264, eds Iyer, H.M. & Hirahara, K., Chapman and Hall, London.

Nolet, G., Van Trier, J. & Huisman, R., 1986. A formalism for non linear inversion of seismic surface waves, *Geophys. Res. Lett.*, **13,** 26–29.

Park, J., 1987. Asymptotic coupled-mode expressions for multiplet amplitude anomalies and frequency shifts on an aspherical Earth, *Geophys. J. R. astr. Soc.*, **90,** 129–169.

Park, J., 1989. Roughness constraints in surface wave tomography, *Geophys. Res. Lett.*, **16,** 1329–1335.

Ritzwoller, M., Masters, G. & Gilbert, F., 1986. Observations of anomalous splitting and their interpretation in terms of aspherical structure, *J. geophys. Res.*, **91,** 10 203–10 228.

Ritzwoller, M., Masters, G. & Gilbert, F., 1988. Constraining aspherical structure with low-degree interaction coefficients: application to uncoupled multiplets, *J. geophys. Res.*, **93,** 6369–6396.

Romanowicz, B., 1987. Multiplet–multiplet coupling due to lateral heterogeneity: asymptotic effects on the amplitude and frequency of the Earth's normal modes, *Geophys. J. R. astr. Soc.*, **90,** 75–100.

Romanowicz, B., 1994. On the measurements of anelastic attenuation using amplitudes of low-frequency surface waves, *Phys. Earth planet. Inter.*, **84,** 179–191.

Stutzmann, E. & Montagner, J.-P., 1993. An inverse technique for retrieving higher mode phase velocity and mantle structure, *Geophys. J. Int.*, **113,** 669–683.

Tanimoto, T., 1984. Waveform inversion of mantle Love waves: the Born seismogram approach, *Geophys. J. R. astr. Soc.*, **78,** 641–660.

Tarantola, A., 1988. Theoretical background for the inversion of seismic waveforms, including elasticity and anelasticity, *Pageoph,* **128,** 365–399.

Tromp, J. & Dalhen, F.A., 1992a. Variational principles for surface wave propagation on a laterally heterogeneous Earth—I. Time-domain JWKB theory, *Geophys. J. Int.*, **109,** 581–598.

Tromp, J. & Dalhen, F.A., 1992b. Variational principles for surface wave propagation on a laterally heterogeneous Earth—II. Frequency-domain JWKB theory, *Geophys. J. Int.*, **109,** 599–619.

Tromp, J. & Dalhen, F.A., 1993. Variational principles for surface wave propagation on a laterally heterogeneous Earth—III. Potential representation, *Geophys. J. Int.*, **112,** 195–209.

Valette, B., 1986. About the influence of pre-stress upon adiabatic perturbation of the earth, *Geophys. J. R. astr. Soc.*, **85,** 179–208.

Woodhouse, J.H., 1983. The joint inversion of seismic waveforms for lateral variations in Earth structure and earthquake source parameters, in *Proc. 'Enrico Fermi' Int. Sch. Phys.*, **LXXXV,** pp. 366–397, eds Kanamori, H. & Boschi, E., North Holland.

Woodhouse, J.H. & Dalhen, F.A., 1978. The effect of a general aspherical perturbation of the free oscillations of the Earth, *Geophys. J. R. astr. Soc.*, **53,** 335–354.

Woodhouse, J.H. & Dziewonski, A.M., 1984. Mapping the upper mantle: three dimensional modelling of earth structure by inversion of seismic waveform, *J. geophys. Res.*, **89,** 5953–5986.

Woodhouse, J.H. & Girnius, T.P., 1982. Surface waves and free oscillations in a regionalized earth model, *Geophys. J. R. astr. Soc.*, **68,** 653–673.

APPENDIX A: TIME-DOMAIN FORMULATION

$\delta\tilde{c}^{(1)}(\sigma)$ has one second-order pole [corresponding to the diagonal terms of $\Lambda^{-1}(\sigma)\Upsilon^{-1}(\sigma)$] and two first-order poles (corresponding to the non-diagonal terms). The time expression of this term can be obtained through inverse Fourier–Laplace transformation, and the kth element of $\delta c^{(1)}(t)$ gives

$$\delta c_1^{(k)}(t) = \frac{-t\exp(i\sigma_k t)}{4\sigma_k^2}\langle \mathbf{v}_k|\delta\mathbf{A}(\sigma_k)|\mathbf{u}_k\rangle\langle \mathbf{v}_k|\mathbf{f}\rangle + \sum_{\substack{k'\\ k'\neq k}} \frac{\exp(i\sigma_k t)}{2i\sigma_k}\frac{1}{\sigma_{k'}^2-\sigma_k^2}\langle \mathbf{v}_k|\delta\mathbf{A}(\sigma_k)|\mathbf{u}_{k'}\rangle\langle \mathbf{v}_{k'}|\mathbf{f}\rangle - \sum_{\substack{k'\\ k'\neq k}} \frac{\exp(i\sigma_{k'} t)}{2i\sigma_{k'}}\frac{1}{\sigma_{k'}^2-\sigma_k^2}\langle \mathbf{v}_k|\delta\mathbf{A}(\sigma_{k'})|\mathbf{u}_{k'}\rangle\langle \mathbf{v}_{k'}|\mathbf{f}\rangle. \tag{A1}$$

This expression gives the displacement contribution of the Fréchet derivative for an impulsive source. In what follows, we will express the acceleration contribution produced by an Heaviside source. We have then to apply two transformations to $\delta\mathbf{c}^{(1)}(t)$: first, a convolution with the Heaviside function $H(t)$, and then a double differentiation, which leads to the expression in acceleration:

second-order pole:

$$-t\exp(i\sigma_k t) \xrightarrow{\text{convol.}H(t)} \frac{1}{\sigma_k}\left[\frac{1}{\sigma_k} + it\exp(i\sigma_k t) - \frac{\exp(i\sigma_k t)}{\sigma_k}\right] \xrightarrow{\text{double deriv.}} -i\sigma_k t\exp(i\sigma_k t),$$

first order pole: (A2)

$$\exp(i\sigma_k t) \xrightarrow{\text{convol.}H(t)} \frac{1}{i\sigma_k}[\exp(i\sigma_k t) - 1] \xrightarrow{\text{double deriv.}} i\sigma_k\exp(i\sigma_k t).$$

We then obtain the following acceleration perturbation:

$$\delta c_k^{(1),\mathrm{acc}}(t) = \frac{-it\exp(\sigma_k t)}{4\sigma_k}\langle \mathbf{v}_k|\boldsymbol{\delta}\mathbf{A}(\sigma_k)|\mathbf{u}_k\rangle\langle \mathbf{v}_k|\mathbf{f}\rangle + \sum_{\substack{k'\\ k'\neq k}} \frac{1}{2}\frac{\exp(i\sigma_k t)}{\sigma_{k'}^2-\sigma_k^2}\langle \mathbf{v}_k|\boldsymbol{\delta}\mathbf{A}(\sigma_k)|\mathbf{u}_{k'}\rangle\langle \mathbf{v}_{k'}|\mathbf{f}\rangle - \sum_{\substack{k'\\ k'\neq k}} \frac{1}{2}\frac{\exp(i\sigma_{k'} t)}{\sigma_{k'}^2-\sigma_k^2}\langle \mathbf{v}_k|\boldsymbol{\delta}\mathbf{A}(\sigma_{k'})|\mathbf{u}_{k'}\rangle\langle \mathbf{v}_{k'}|\mathbf{f}\rangle. \quad \text{(A3)}$$

We then use another approximation, by considering the perturbation $\boldsymbol{\delta}\mathbf{A}$ as a perturbation around the central frequency of the multiplet associated with the singlet where the perturbation is taken. For a singlet k of the multiplet K, the mean frequency σ_K is related to σ_k by $\sigma_k = \sigma_K + \delta\sigma_k$ (idem for k' and the corresponding multiplet K'), so that we take

$$\boldsymbol{\delta}\mathbf{A}(\sigma_k) \simeq \boldsymbol{\delta}\mathbf{A}(\sigma_K) + (\sigma_k - \sigma_K)\partial_\sigma \boldsymbol{\delta}\mathbf{A}(\sigma_K), \quad \text{(A4)}$$

$$\boldsymbol{\delta}\mathbf{A}(\sigma_{k'}) \simeq \boldsymbol{\delta}\mathbf{A}(\sigma_{K'}) + (\sigma_{k'} - \sigma_{K'})\partial_\sigma \boldsymbol{\delta}\mathbf{A}(\sigma_{K'}), \quad \text{(A5)}$$

and $\delta c_k^{(1),\mathrm{acc}}(t)$ becomes

$$\begin{aligned}\delta c_k^{(1),\mathrm{acc}}(t) = {} & \frac{-it}{4\sigma_k}\exp(i\sigma_k t)\langle \mathbf{v}_k|\boldsymbol{\delta}\mathbf{A}(\sigma_K)|\mathbf{u}_k\rangle\langle \mathbf{v}_k|\mathbf{f}\rangle \\ & + \sum_{\substack{k'\\ k'\neq k}} \frac{1}{2}\frac{1}{\sigma_{k'}^2-\sigma_k^2}\exp(i\sigma_k t)\langle \mathbf{v}_k|\boldsymbol{\delta}\mathbf{A}(\sigma_K)|\mathbf{u}_{k'}\rangle\langle \mathbf{v}_{k'}|\mathbf{f}\rangle \\ & - \sum_{\substack{k'\\ k'\neq k}} \frac{1}{2}\frac{1}{\sigma_{k'}^2-\sigma_k^2}\exp(i\sigma_{k'} t)\langle \mathbf{v}_k|\boldsymbol{\delta}\mathbf{A}(\sigma_{K'})|\mathbf{u}_{k'}\rangle\langle \mathbf{v}_{k'}|\mathbf{f}\rangle \\ & - \frac{it(\sigma_k-\sigma_K)}{4\sigma_k}\exp(i\sigma_k t)\langle \mathbf{v}_k|\partial_\sigma\boldsymbol{\delta}\mathbf{A}(\sigma_K)|\mathbf{u}_k\rangle\langle \mathbf{v}_k|\mathbf{f}\rangle \\ & + \sum_{\substack{k'\\ k'\neq k}} \frac{1}{2}\frac{\sigma_k-\sigma_K}{\sigma_{k'}^2-\sigma_k^2}\exp(i\sigma_k t)\langle \mathbf{v}_k|\partial_\sigma\boldsymbol{\delta}\mathbf{A}(\sigma_K)|\mathbf{u}_{k'}\rangle\langle \mathbf{v}_{k'}|\mathbf{f}\rangle \\ & - \sum_{\substack{k'\\ k'\neq k}} \frac{1}{2}\frac{\sigma_{k'}-\sigma_{K'}}{\sigma_{k'}^2-\sigma_k^2}\exp(i\sigma_k t) \\ & \times \langle \mathbf{v}_k|\partial_\sigma\boldsymbol{\delta}\mathbf{A}(\sigma_{K'})|\mathbf{u}_{k'}\rangle\langle \mathbf{v}_{k'}|\mathbf{f}\rangle. \end{aligned} \quad \text{(A6)}$$

APPENDIX B: SELF-COUPLING CONTRIBUTION

The contribution of the self-coupling part is given by

$$\begin{aligned}\delta s_{K,K}(t) = \sum_{k\in K}\langle \mathbf{R}|\mathbf{u}_k\rangle\Bigg[& \frac{-it}{4\sigma_k}\exp(i\sigma_k t)\langle \mathbf{v}_k|\boldsymbol{\delta}\mathbf{A}(\sigma_K)|\mathbf{u}_k\rangle\langle \mathbf{v}_k|\mathbf{f}\rangle \\ & + \sum_{k'\neq k}\frac{1}{2}\frac{1}{\sigma_{k'}^2-\sigma_k^2}[\exp(i\sigma_k t)-\exp(i\sigma_{k'} t)] \\ & \times \langle \mathbf{v}_k|\boldsymbol{\delta}\mathbf{A}(\sigma_K)|\mathbf{u}_{k'}\rangle\langle \mathbf{v}_{k'}|\mathbf{f}\rangle \\ & + \sum_{k'\neq k}\frac{1}{4}\frac{1}{\sigma_{k'}^2-\sigma_k^2}\{(\sigma_k-\sigma_{k'})[\exp(i\sigma_k t)+\exp(i\sigma_{k'} t)] \\ & + \delta\sigma_k[\exp(i\sigma_k t)-\exp(i\sigma_{k'} t)] \\ & + \delta\sigma_{k'}[\exp(i\sigma_k t)-\exp(i\sigma_{k'} t)]\} \\ & \times \langle \mathbf{v}_k\partial_\sigma\boldsymbol{\delta}\mathbf{A}(\sigma_K)|\mathbf{u}_{k'}\rangle\langle \mathbf{v}_{k'}|\mathbf{f}\rangle\Bigg]. \end{aligned} \quad \text{(B1)}$$

Employing the equality

$$\begin{aligned}\frac{1}{\sigma_{k'}^2-\sigma_k^2}[\exp(i\sigma_k t)-\exp(i\sigma_{k'} t)] &= \frac{-i}{\sigma_{k'}+\sigma_k}\exp(i\sigma_k t)\int_0^t \exp[i(\sigma_{k'}-\sigma_k)\tau]\,d\tau \\ &= \frac{-i}{\sigma_{k'}+\sigma_k}\exp(i\sigma_K t)\int_0^t \exp[i\sigma_k(t-\tau)]\exp(i\sigma_{k'}\tau)\,d\tau, \end{aligned} \quad \text{(B2)}$$

and the approximation

$$\begin{aligned}\frac{1}{\sigma_{k'}+\sigma_k} &\simeq \frac{1}{2\sigma_K}\left(1+\frac{\delta\sigma_{k'}+\delta\sigma_k}{2\sigma_K}\right)^{-1} \\ &\simeq \frac{1}{2\sigma_K}\left(1-\frac{\delta\sigma_{k'}}{2\sigma_K}-\frac{\delta\sigma_k}{2\sigma_K}\right), \end{aligned} \quad \text{(B3)}$$

we can then express the contribution of all the singlets of the multiplet by using the expressions (11) and (13). We thus obtain

$$\begin{aligned}\delta s_{K,K}(t) = \exp(i\sigma_K t)\Bigg\{ & \frac{-i}{4\sigma_K}\int_0^t \langle \mathbf{R}_K(t-\tau)|\boldsymbol{\delta}\mathbf{A}(\sigma_K)|\mathbf{S}_K(\tau)\rangle\,d\tau \\ & + \frac{1}{8\sigma_K^2}\int_0^t [\langle \dot{\mathbf{R}}_K(t-\tau)|\boldsymbol{\delta}\mathbf{A}(\sigma_K)|\mathbf{S}_K(\tau)\rangle \\ & + \langle \mathbf{R}_K(t-\tau)|\boldsymbol{\delta}\mathbf{A}(\sigma_K)|\dot{\mathbf{S}}_K(\tau)\rangle]\,d\tau \\ & - \frac{1}{8\sigma_K}\int_0^t [\langle \dot{\mathbf{R}}_K(t-\tau)|\partial_\sigma\boldsymbol{\delta}\mathbf{A}(\sigma_K)|\mathbf{S}_K(\tau)\rangle \\ & + \langle \mathbf{R}_K(t-\tau)|\partial_\sigma\boldsymbol{\delta}\mathbf{A}(\sigma_K)|\dot{\mathbf{S}}_K(\tau)\rangle]\,d\tau \\ & - \frac{1}{8\sigma_K}[\langle \mathbf{R}_K(t)|\partial_\sigma\boldsymbol{\delta}\mathbf{A}(\sigma_K)|\mathbf{S}_K(0)\rangle \\ & + \langle \mathbf{R}_K(0)|\partial_\sigma\boldsymbol{\delta}\mathbf{A}(\sigma_K)|\mathbf{S}_K(t)\rangle] \\ & - \frac{i}{16\sigma_K^2}[\langle \dot{\mathbf{R}}_K(t)|\partial_\sigma\boldsymbol{\delta}\mathbf{A}(\sigma_K)|\mathbf{S}_K(0)\rangle \\ & + \langle \dot{\mathbf{R}}_K(0)|\partial_\sigma\boldsymbol{\delta}\mathbf{A}(\sigma_K)|\mathbf{S}_K(t)\rangle] \\ & - \frac{i}{16\sigma_K^2}[\langle \mathbf{R}_K(t)|\partial_\sigma\boldsymbol{\delta}\mathbf{A}(\sigma_K)|\dot{\mathbf{S}}_K(0)\rangle \\ & + \langle \mathbf{R}_K(0)|\partial_\sigma\boldsymbol{\delta}\mathbf{A}(\sigma_K)|\dot{\mathbf{S}}_K(t)\rangle]\Bigg\}, \end{aligned} \quad \text{(B4)}$$

where $\langle \dot{\mathbf{R}}_K(t)|$ and $|\dot{\mathbf{S}}_K(t)\rangle$ are the time derivatives of $\langle \mathbf{R}_K(t)|$ and $|\mathbf{S}_K(t)\rangle$ respectively.

APPENDIX C: COUPLING BETWEEN DIFFERENT MULTIPLETS

If we consider the case of a weak splitting, we can make the approximation

$$\begin{aligned}\frac{1}{\sigma_{k'}^2-\sigma_k^2} &\simeq \frac{1}{\sigma_{K'}^2-\sigma_K^2}\left(1+\frac{\delta\sigma_{k'}+\delta\sigma_k}{\sigma_{K'}+\sigma_K}\right)^{-1}\left(1+\frac{\delta\sigma_{k'}-\delta\sigma_k}{\sigma_{K'}-\sigma_K}\right)^{-1} \\ &\simeq \frac{2}{\sigma_{K'}^2-\sigma_K^2}\left(1-\frac{2\sigma_{K'}}{\sigma_{K'}^2-\sigma_K^2}\delta\sigma_{k'}+\frac{2\sigma_K}{\sigma_{K'}^2-\sigma_K^2}\delta\sigma_k\right). \end{aligned}$$

Thus, as we have done previously, we obtain an expression of the non-dispersive part of the complex signal (in acceleration) corresponding to the coupling between multiplets, with the weak-splitting approximation:

$$\begin{aligned}\delta s_{K,K'}(t) = &\frac{\exp(i\sigma_K t)}{\sigma_{K'}^2 - \sigma_K^2}[\langle \mathbf{R}_K(t)|\delta\mathbf{A}(\sigma_K)|\mathbf{S}_{K'}(0)\rangle \\ &+ i\langle \dot{\mathbf{R}}_K(t)|\partial_\sigma \delta\mathbf{A}(\sigma_K)|\mathbf{S}_{K'}(0)\rangle] \\ &+ \frac{\exp(i\sigma_K t)}{(\sigma_{K'}^2 - \sigma_K^2)^2}[2i\sigma_{K'}\langle \mathbf{R}_K(t)|\delta\mathbf{A}(\sigma_K)|\dot{\mathbf{S}}_{K'}(0)\rangle \\ &- 2i\sigma_K\langle \dot{\mathbf{R}}_K(t)|\delta\mathbf{A}(\sigma_K)|\mathbf{S}_{K'}(0)\rangle] \\ &- \frac{\exp(i\sigma_{K'} t)}{\sigma_{K'}^2 - \sigma_K^2}[\langle \mathbf{R}_K(0)|\delta\mathbf{A}(\sigma_{K'})|\mathbf{S}_{K'}(t)\rangle \\ &+ i\langle \mathbf{R}_K(0)|\partial_\sigma \delta\mathbf{A}(\sigma_{K'})|\dot{\mathbf{S}}_{K'}(t)\rangle] \\ &- \frac{\exp(i\sigma_{K'} t)}{(\sigma_{K'}^2 - \sigma_K^2)^2}[2i\sigma_{K'}\langle \mathbf{R}_K(0)|\delta\mathbf{A}(\sigma_{K'})|\dot{\mathbf{S}}_{K'}(t)\rangle \\ &- 2i\sigma_K\langle \dot{\mathbf{R}}_K(0)|\delta\mathbf{A}(\sigma_{K'})|\mathbf{S}_{K'}(t)\rangle]. \qquad \text{(C1)}\end{aligned}$$